

**CHAPTER 4 «FOCUSING LASER BEAMS  
WITH DIFFERENT TYPES  
OF SPATIAL POLARIZATION OF RADIATION»**

DOI: <https://doi.org/10.30525/978-9934-26-461-0-4>

Terahertz (THz) laser beams can be used to diagnose thin films and material surfaces, study biological objects, and achieve subwavelength resolution in tomography, as well as in information transmission and processing systems, communication systems, image processing, and lithography. Recently, considerable attention has been paid to radial and azimuthal polarized laser radiation. In a number of articles, it is shown that such radiation has a significant prospect of application in the creation of optomagnetic devices, can improve the configuration of the focal spot, reduce the focal length, and achieve a greater depth of focus [144; 145].

In the visible range, the physical principles of focusing laser beams with nonuniform spatial polarization of radiation are established [146], the possibility of forming and controlling light fields with subwavelength energy localization regions is shown. For the THz range, the focusing properties of laser beams with nonuniform spatial polarization have been studied only in a small number of articles. The radiation of milliwatt generators of subpicosecond broadband pulses of femtosecond lasers was studied in these works. This approach leads to rather high complexity of manufacturing laser systems. For expansion the possibilities of scientific and technical applications, the study of intensity distributions in the focal region of the focusing system with different types of nonuniform spatial polarization of continuous THz radiation is relevant.

This chapter presents the results of theoretical and experimental studies of the patterns of focusing of transverse modes with spatially nonuniform polarization in dielectric and metal resonators of a THz laser.

**4.1. FOCUSING OF LOWER-ORDER MODES  
OF TERAHERTZ LASER BASED ON A HOLLOW  
DIELECTRIC CIRCULAR WAVEGUIDE**

**4.1.1. Theoretical Relationships**

The free space propagation of laser radiation along the  $Oz$  axis is described by the well-known Rayleigh-Sommerfeld integrals in the nonparaxial

approximation [142]. These integrals in the cylindrical coordinate system have the following form:

$$\left\{ \begin{array}{l}
 E_r(\rho, \theta, z) = -\frac{ikz}{2\pi\xi^3} \exp(ik\xi) \int_0^\infty \int_0^{2\pi} [E_r(r, \phi + \theta, 0) \cos\phi - \\
 \quad - E_\phi(r, \phi + \theta, 0) \sin\phi] \exp\left(\frac{ikr^2}{2\xi}\right) \exp(-i\gamma r \cos\phi) r dr d\phi, \\
 E_\phi(\rho, \theta, z) = -\frac{ikz}{2\pi\xi^2} \exp(ik\xi) \int_0^\infty \int_0^{2\pi} [E_r(r, \phi + \theta, 0) \sin\phi + \\
 \quad + E_\phi(r, \phi + \theta, 0) \cos\phi] \exp\left(\frac{ikr^2}{2\xi}\right) \exp(-i\gamma r \cos\phi) r dr d\phi, \\
 E_z(\rho, \theta, z) = \frac{ik}{2\pi\xi^2} \exp(ik\xi) \int_0^\infty \int_0^{2\pi} [E_r(r, \phi + \theta, 0)(r - \rho \cos\phi) + \\
 \quad + E_\phi(r, \phi + \theta, 0) \rho \sin\phi] \exp\left(\frac{ikr^2}{2\xi}\right) \exp(-i\gamma r \cos\phi) r dr d\phi,
 \end{array} \right. \quad (4.1)$$

where  $k = 2\pi/\lambda$  is the wave number;  $\lambda$  is the wavelength;  $\rho, \theta, z$  are the cylindrical coordinates in the observation plane;  $r$  and  $\phi$  are the polar coordinates in the area of definition of the initial field;  $\xi = \sqrt{z^2 + \rho^2}$ ;  $\gamma = k\rho/\xi$ .

The modes of the investigated laser resonator, used for focusing radiation, coincide with the modes of a circular dielectric waveguide. Let radiation be given in the form of symmetric azimuthally and radially polarized radiation in the initial plane  $TE_{01}$ ,  $TM_{01}$ , and asymmetric linearly polarized  $EH_{11}$  and  $TE_{01} + EH_{21}$  modes of a circular hollow dielectric waveguide with a radius  $a_1$  (Figure 4.1).

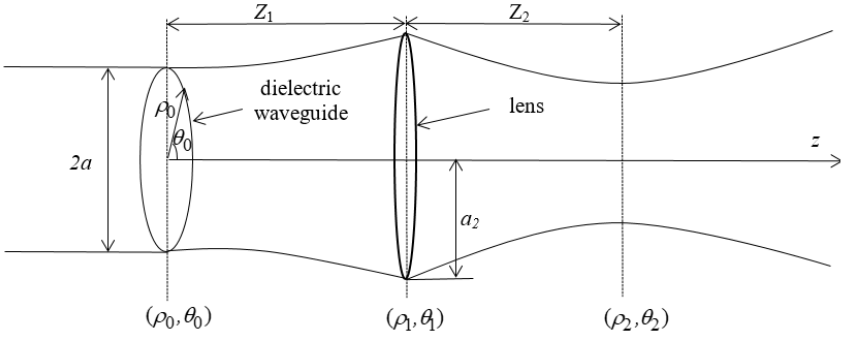


Figure 4.1. Theoretical scheme of the calculation model

The normalized components of the electric fields in the source plane (on the output mirror of the laser) for these modes have the form [50]:

$$\text{TE}_{01} \text{ mode:} \quad \begin{cases} \bar{E}_r(r, \phi) = 0, \\ \bar{E}_\phi(r, \phi) = A_{01} J_1 \left( \chi_{01} \frac{r}{a_1} \right), \end{cases} \quad (4.2)$$

$$\text{TM}_{01} \text{ mode:} \quad \begin{cases} \bar{E}_r(r, \phi) = B_{01} J_1 \left( \chi_{01} \frac{r}{a_1} \right), \\ \bar{E}_\phi(r, \phi) = 0, \end{cases} \quad (4.3)$$

$$\text{EH}_{11} \text{ mode:} \quad \begin{cases} \bar{E}_r(r, \phi) = C_{11} J_0 \left( \chi_{11} \frac{r}{a_1} \right) \sin(\phi), \\ \bar{E}_\phi(r, \phi) = C_{11} J_0 \left( \chi_{11} \frac{r}{a_1} \right) \cos(\phi), \end{cases} \quad (4.4)$$

$$\text{TE}_{01} + \text{EH}_{21} \text{ mode:} \quad \begin{cases} \bar{E}_r(r, \phi) = D_{21} J_1 \left( \chi_{01} \frac{r}{a_1} \right) \sin(2\phi), \\ \bar{E}_\phi(r, \phi) = D_{21} J_1 \left( \chi_{01} \frac{r}{a_1} \right) \cos(1 + 2\phi), \end{cases} \quad (4.5)$$

where  $A_{01} = \frac{1}{a_1 \sqrt{\pi} \chi_{01} J_0(\chi_{01})}$ ,  $B_{01} = \frac{1}{a_1 \sqrt{\pi} J_2(\chi_{01})}$ ,  $C_{11} = \frac{1}{a_1 \sqrt{\pi} J_1(\chi_{11})}$ ,  
 $D_{21} = \frac{\sqrt{2}}{2a_1 \sqrt{\pi} J_2(\chi_{21})}$  are the normalizing factors;  $J_0, J_1, J_2$  are the Bessel

functions of the first order;  $\chi_{01}, \chi_{11}, \chi_{21}$  are the roots of the equation  $J_1(\chi) = 0$ .

Using the expressions for the field components, for example  $TM_{01}$ -mode (4.3) and applying the integral Rayleigh-Sommerfeld transformations (4.1) to them, we obtain the expressions for the field components of this mode in free space at a distance  $z_1$  from the end of the waveguide:

$$\left\{ \begin{array}{l} E_{r_1}(\rho_1, \theta_1, z_1) = -\frac{kz_1}{\xi_1^2} \exp(ik\xi_1) B_{01} \int_0^{a_1} J_1\left(\chi_{01} \frac{r}{a_1}\right) J_1(\gamma_1 r) \exp\left(\frac{ikr^2}{2\xi_1}\right) r dr, \\ E_{\phi_1}(\rho_1, \theta_1, z_1) = 0, \\ E_{z_1}(\rho_1, \theta_1, z_1) = \frac{ik}{\xi_1^2} \exp(ik\xi_1) B_{01} \int_0^{a_1} J_1\left(\chi_{01} \frac{r}{a_1}\right) \left[ rJ_0(\gamma_1 r) + i\rho J_1(\gamma_1 r) \right] \times \\ \quad \times \exp\left(\frac{ikr^2}{2\xi_1}\right) r dr, \end{array} \right. \quad (4.6)$$

where  $\xi_1 = \sqrt{z_1^2 + \rho_1^2}$ ,  $\gamma_1 = k\rho_1 / \xi_1$ .

The field at the entrance and exit of the lens with radius  $a_2$  will be described using the phase correction function  $Ph(\rho_1) = \exp\left(\frac{-i\pi\rho_1^2}{\lambda F}\right)$ , where  $F$  is the focal length of the lens [148]. By again applying the integral Rayleigh-Sommerfeld transformations (4.1) to the components of the electric field strength vector (4.6) found after phase correction, we obtain analytical expressions for the transverse and longitudinal field components of the  $TM_{01}$  mode at a distance  $z_2$  from the lens:

$$\left\{ \begin{aligned}
 E_r(\rho_2, \theta_2, z_2) &= \frac{k^2 z_1 z_2}{\xi_2^2} \exp(ik\xi_2) B_{01} \int_0^{a_2} \frac{\exp(ik\xi_1)}{\xi_1^2} \int_0^{a_1} J_1\left(\chi_{01} \frac{r}{a_1}\right) J_1(\gamma_1 r) \times \\
 &\quad \times \exp\left(\frac{ikr^2}{2\xi_1}\right) r dr J_1(\gamma_2 \rho_1) \exp\left(\frac{ik\rho_1^2}{2\xi_2}\right) Ph(\rho_1) \rho_1 d\rho_1, \\
 E_\phi(\rho_2, \theta_2, z_2) &= 0, \\
 E_z(\rho_2, \theta_2, z_2) &= \frac{ik^2 z_1}{\xi_2^2} \exp(ik\xi_2) B_{01} \int_0^{a_2} \frac{\exp(ik\xi_1)}{\xi_1^2} \int_0^{a_1} J_1\left(\chi_{01} \frac{r}{a_1}\right) J_1(\gamma_1 r) \times \\
 &\quad \times \exp\left(\frac{ikr^2}{2\xi_1}\right) r dr [\rho_1 J_0(\gamma_2 \rho_1) + i\rho_2 J_1(\gamma_2 \rho_1)] \exp\left(\frac{ik\rho_1^2}{2\xi_2}\right) Ph(\rho_1) \rho_1 d\rho_1,
 \end{aligned} \right. \quad (4.7)$$

where  $\rho_2, \theta_2, z_2$  are the cylindrical coordinates in the lens observation plane;  $\xi_2 = \sqrt{z_2^2 + \rho_2^2}$ ,  $\gamma_2 = k\rho_2 / \xi_2$ . Similarly, expressions for all components of the electric field strength vector were obtained for  $TE_{01}$ ,  $EH_{11}$  and  $TE_{01} + EH_{21}$  modes in the observation plane.

The field components for an azimuthally polarized symmetric  $TE_{01}$  mode at a distance  $z_2$  from the lens have the form:

$$\left\{ \begin{aligned}
 E_r(\rho_2, \theta_2, z_2) &= 0, \\
 E_\phi(\rho_2, \theta_2, z_2) &= -\frac{k^2 z_1 z_2}{\xi_2^2} \exp(ik\xi_2) A_{01} \int_0^{a_2} \frac{\exp(ik\xi_1)}{\xi_1^2} \int_0^{a_1} J_1\left(\chi_{01} \frac{r}{a_1}\right) \times \\
 &\quad \times J_1(\gamma_1 r) \exp\left(\frac{ikr^2}{2\xi_1}\right) r dr J_1(\gamma_2 \rho_1) \exp\left(\frac{ik\rho_1^2}{2\xi_2}\right) Ph(\rho_1) \rho_1 d\rho_1, \\
 E_z(\rho_2, \theta_2, z_2) &= 0.
 \end{aligned} \right. \quad (4.8)$$

The field components for linearly polarized  $EH_{11}$  and  $TE_{01} + EH_{21}$  modes at a distance  $z_2$  from the lens have the form:

$$\left. \begin{aligned}
 E_r(\rho_2, \theta_2, z_2) &= \frac{k^2 z_1 z_2}{\xi_2^2} \exp(ik\xi_2) \sin(\theta_2) C_{11} \int_0^{a_2} \frac{\exp(ik\xi_1)}{\xi_1^2} \times \int_0^{a_1} J_0\left(\chi_{01} \frac{r}{a_1}\right) \times \\
 &\quad \times J_0(\gamma_1 r) \exp\left(\frac{ikr^2}{2\xi_1}\right) r dr J_0(\gamma_2 \rho_1) \exp\left(\frac{ik\rho_1^2}{2\xi_2}\right) Ph(\rho_1) \rho_1 d\rho_1, \\
 E_\phi(\rho_2, \theta_2, z_2) &= \frac{k^2 z_1 z_2}{\xi_2^2} \exp(ik\xi_2) \cos(\theta_2) C_{11} \int_0^{a_2} \frac{\exp(ik\xi_1)}{\xi_1^2} \int_0^{a_1} J_0\left(\chi_{01} \frac{r}{a_1}\right) \times \\
 &\quad \times J_0(\gamma_1 r) \exp\left(\frac{ikr^2}{2\xi_1}\right) r dr J_0(\gamma_2 \rho_1) \exp\left(\frac{ik\rho_1^2}{2\xi_2}\right) Ph(\rho_1) \rho_1 d\rho_1, \\
 E_z(\rho_2, \theta_2, z_2) &= \frac{ik^2 z_1}{\xi_2^2} \exp(ik\xi_2) \sin(\theta_2) C_{11} \int_0^{a_2} \frac{\exp(ik\xi_1)}{\xi_1^2} \int_0^{a_1} J_0\left(\chi_{01} \frac{r}{a_1}\right) \times \\
 &\quad \times J_0(\gamma_1 r) \exp\left(\frac{ikr^2}{2\xi_1}\right) r dr \times [i\rho_1 J_1(\gamma_2 \rho_1) + \rho_2 J_1(\gamma_2 \rho_1)] \times \\
 &\quad \times \exp\left(\frac{ik\rho_1^2}{2\xi_2}\right) Ph(\rho_1) \rho_1 d\rho_1. \\
 E_r(\rho_2, \theta_2, z_2) &= \frac{-ik^2 z_1 z_2}{\xi_2^2} \exp(ik\xi_2) \sin(\theta_2) D_{21} \int_0^{a_2} \frac{\exp(ik\xi_1)}{\xi_1^2} \times \\
 &\quad \times \int_0^{a_1} J_1\left(\chi_{01} \frac{r}{a_1}\right) J_1(\gamma_1 r) \exp\left(\frac{ikr^2}{2\xi_1}\right) r dr J_1(\gamma_2 \rho_1) \exp\left(\frac{ik\rho_1^2}{2\xi_2}\right) Ph(\rho_1) \rho_1 d\rho_1, \\
 E_\phi(\rho_2, \theta_2, z_2) &= \frac{-ik^2 z_1 z_2}{\xi_2^2} \exp(ik\xi_2) \cos(\theta_2 + 1) D_{21} \int_0^{a_2} \frac{\exp(ik\xi_1)}{\xi_1^2} \times \\
 &\quad \times \int_0^{a_1} J_1\left(\chi_{01} \frac{r}{a_1}\right) J_1(\gamma_1 r) \exp\left(\frac{ikr^2}{2\xi_1}\right) r dr J_1(\gamma_2 \rho_1) \exp\left(\frac{ik\rho_1^2}{2\xi_2}\right) Ph(\rho_1) \rho_1 d\rho_1, \\
 E_z(\rho_2, \theta_2, z_2) &= \frac{ik^2 z_1}{\xi_2^2} \exp(ik\xi_2) \sin(\theta_2) D_{21} \int_0^{a_2} \frac{\exp(ik\xi_1)}{\xi_1^2} \int_0^{a_1} J_1\left(\chi_{01} \frac{r}{a_1}\right) \times \\
 &\quad \times J_1(\gamma_1 r) \exp\left(\frac{ikr^2}{2\xi_1}\right) r dr [\rho_1 J_2(\gamma_2 \rho_1) - i\rho_2 J_1(\gamma_2 \rho_1)] \\
 &\quad \times \exp\left(\frac{ik\rho_1^2}{2\xi_2}\right) Ph(\rho_1) \rho_1 d\rho_1.
 \end{aligned} \right\} \quad (4.9)$$

$$\left. \begin{aligned}
 E_r(\rho_2, \theta_2, z_2) &= \frac{-ik^2 z_1 z_2}{\xi_2^2} \exp(ik\xi_2) \sin(\theta_2) D_{21} \int_0^{a_2} \frac{\exp(ik\xi_1)}{\xi_1^2} \times \\
 &\quad \times \int_0^{a_1} J_1\left(\chi_{01} \frac{r}{a_1}\right) J_1(\gamma_1 r) \exp\left(\frac{ikr^2}{2\xi_1}\right) r dr J_1(\gamma_2 \rho_1) \exp\left(\frac{ik\rho_1^2}{2\xi_2}\right) Ph(\rho_1) \rho_1 d\rho_1, \\
 E_\phi(\rho_2, \theta_2, z_2) &= \frac{-ik^2 z_1 z_2}{\xi_2^2} \exp(ik\xi_2) \cos(\theta_2 + 1) D_{21} \int_0^{a_2} \frac{\exp(ik\xi_1)}{\xi_1^2} \times \\
 &\quad \times \int_0^{a_1} J_1\left(\chi_{01} \frac{r}{a_1}\right) J_1(\gamma_1 r) \exp\left(\frac{ikr^2}{2\xi_1}\right) r dr J_1(\gamma_2 \rho_1) \exp\left(\frac{ik\rho_1^2}{2\xi_2}\right) Ph(\rho_1) \rho_1 d\rho_1, \\
 E_z(\rho_2, \theta_2, z_2) &= \frac{ik^2 z_1}{\xi_2^2} \exp(ik\xi_2) \sin(\theta_2) D_{21} \int_0^{a_2} \frac{\exp(ik\xi_1)}{\xi_1^2} \int_0^{a_1} J_1\left(\chi_{01} \frac{r}{a_1}\right) \times \\
 &\quad \times J_1(\gamma_1 r) \exp\left(\frac{ikr^2}{2\xi_1}\right) r dr [\rho_1 J_2(\gamma_2 \rho_1) - i\rho_2 J_1(\gamma_2 \rho_1)] \\
 &\quad \times \exp\left(\frac{ik\rho_1^2}{2\xi_2}\right) Ph(\rho_1) \rho_1 d\rho_1.
 \end{aligned} \right\} \quad (4.10)$$

**4.1.2. Calculation Results and Their Analysis**

Using the expressions obtained in 4.1.1, calculations of the total field intensity of the studied modes  $I = |E_r|^2 + |E_\phi|^2 + |E_z|^2$ , were carried out as well as the intensity of their longitudinal components in the focal region of the lens. The wavelength of the investigated radiation was 0.4326 mm (the generation line of a THz laser with optical pumping on the HCOOH molecule). The diameter of the waveguide was chosen equal to  $2a_1 = 35$  mm, and the diameter of the lens was  $2a_2 = 50$  mm. The focal length of the lens  $F = 36.36$  mm was chosen according to the conditions of sharp (numerical aperture of the lens [147]  $NA = 0.68$ , where  $NA = a_2/F$ ) and  $F = 160$  mm according to the conditions of moderate focus ( $NA = 0.16$ ). For complete interception of the beam, the distance  $z_1$  was chosen equal to 300 mm.

Figures 4.2–4.3 show the distributions of the total field intensity of the radially polarized  $TM_{01}$  mode and the intensity of its longitudinal component at moderate and at sharp focusing in the focal region of the lens. The total field intensity of this mode is determined by only two components –  $E_r$  and  $E_z$ .

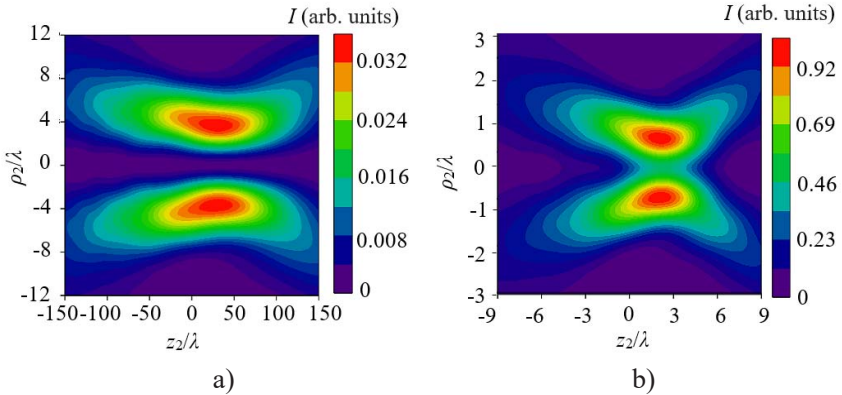


**Figure 4.2** Calculated distributions of the total  $TM_{01}$  mode field intensity at moderate (a) and at sharp (b) focusing in the focal region of the lens

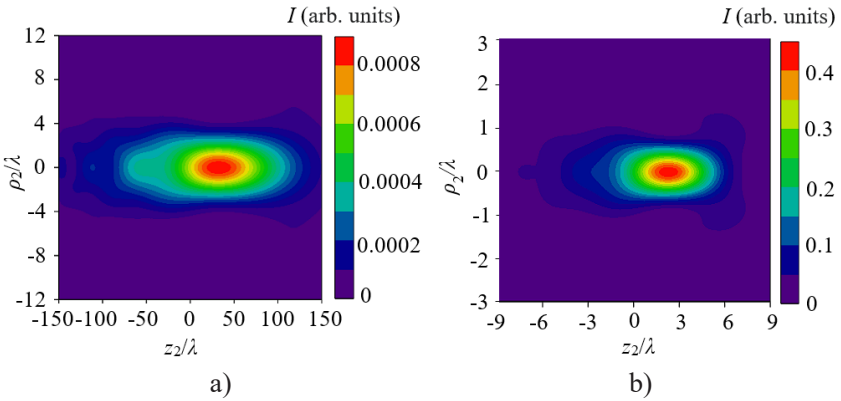


**Figure 4.3** Calculated distributions of the intensity of the longitudinal component of the  $TM_{01}$ -mode field at moderate (a) and at sharp (b) focusing in the focal region of the lens

It can be seen from the figures that when the radiation is sharply focused, there is a significant increase in the axial intensity in the field distribution (Figure 3.2, b). However, this increase is absent at moderate focusing (Figure 3.2, a). This is due to the fact that the longitudinal component of the field during sharp focusing makes a significant contribution to the overall intensity of this mode (Figure 4.3, b). The maximum value of the total field intensity of this mode is 29 times higher at sharp than at moderate focusing. At the same time, the diameter of the  $TM_{01}$  mode beam at the focus of the lens at half of the intensity FWHM (full width at half maximum) at moderate focusing is equal  $11.9 \lambda$ , and at sharp focusing is  $FWHM = 2.7 \lambda$ .

The distribution of the total field intensity of the azimuthally polarized  $TE_{01}$  mode of the dielectric resonator in the focal region of the lens retains a ring-like appearance (Figure 4.4) both at moderate and at sharp focusing. The total intensity of this mode is determined by only one transverse angular component (4.8). The diameter of the beam of this mode at the focus of the lens at moderate focusing is  $FWHM = 10.8 \lambda$ , and at sharp focusing is  $FWHM = 2.5 \lambda$ . The maximum value of the total intensity of the  $TE_{01}$  mode field, as well as the  $TM_{01}$  mode, increases 30 times at sharp focusing compared to moderate focusing.

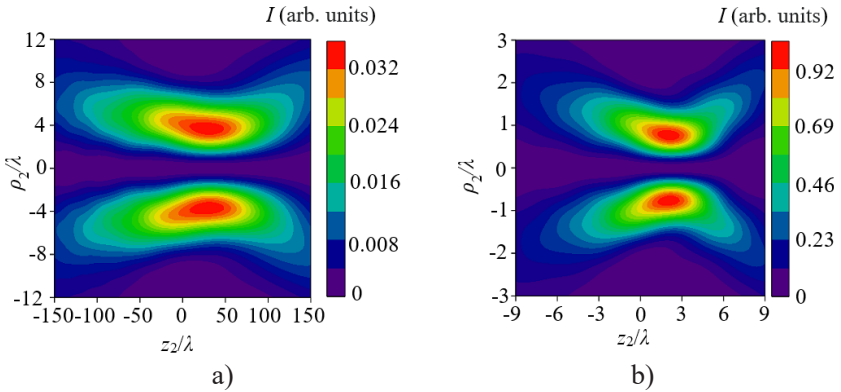


**Figure 4.4. Calculated distributions of the total  $TE_{01}$  mode field intensity at moderate (a) and at sharp (b) focusing in the focal region of the lens**

Figures 4.5 – 4.6 show the distributions of the total field intensity and the intensity of its longitudinal component for the linearly polarized  $EH_{11}$  mode.

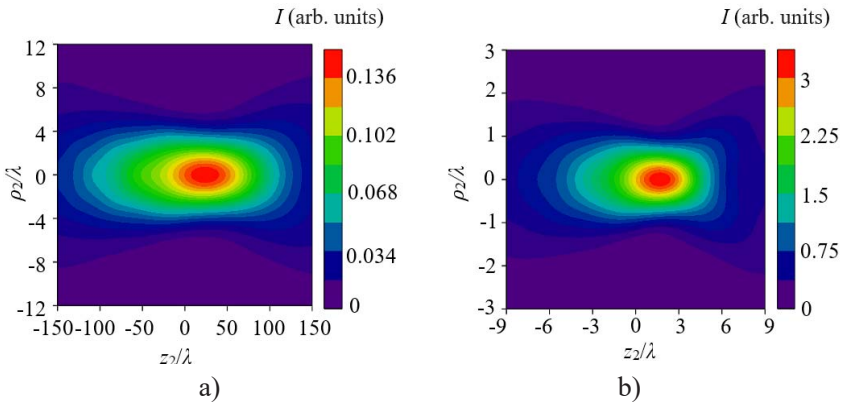


**Figure 4.5. Estimated distributions of the total intensity of the  $EH_{11}$  mode field at moderate (a) and at sharp (b) focusing in the focal region of the lens**

The total field intensity of the  $\text{EH}_{11}$  mode in the center of the focal spot has a maximum (Figure 4.5) and it is 22 times higher at sharp focusing than at moderate focusing.

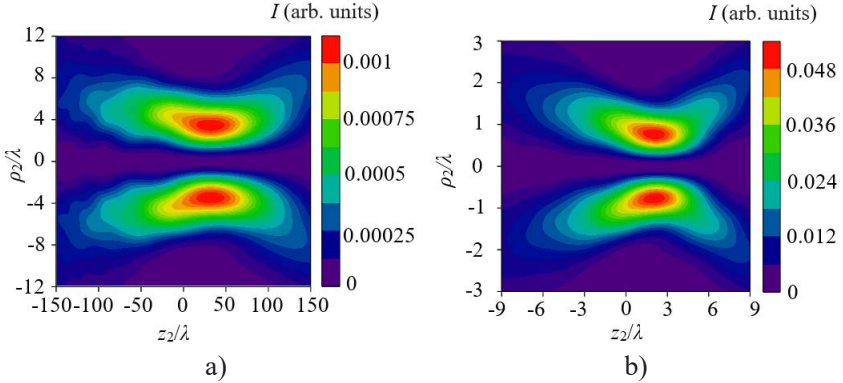


**Figure 4.6. Calculated intensity distributions of the longitudinal component of the  $\text{EH}_{11}$  mode field at moderate (a) and at sharp (b) focusing in the focal region of the lens**

Beam diameter for the  $\text{EH}_{11}$  mode in the lens focus at moderate focusing is  $\text{FWHM} = 5.1 \lambda$ , while at sharp focusing is  $\text{FWHM} = 1.2 \lambda$ . At the same time, the total field intensity of this mode is determined by all three components. A dip is observed in the field distribution for the longitudinal component of the  $\text{EH}_{11}$  mode in the focal region of the lens (Figure 4.6), but the contribution of this component to the total intensity is insignificant.

For the linearly polarized  $\text{TE}_{01} + \text{EH}_{21}$  mode in the focal region of the lens, the transverse distribution of the total field intensity has a dip both at sharp and moderate focusing (Figure 4.7). The maximum value of the total field intensity of this mode at sharp focusing exceeds the maximum value at moderate by 18 times. The total field intensity of this mode, as well as for the  $\text{EH}_{11}$  mode, is determined by all three components. At the same time, the beam diameter of the  $\text{TE}_{01} + \text{EH}_{21}$  mode at the focus of the lens at moderate focusing is  $\text{FWHM} = 13.18 \lambda$ , while at sharp focusing is  $\text{FWHM} = 3.00 \lambda$ .

A dip is also observed in the field distribution for the longitudinal component of the  $TE_{01}+EH_{21}$  mode in the focal region of the lens (Figure 4.8).

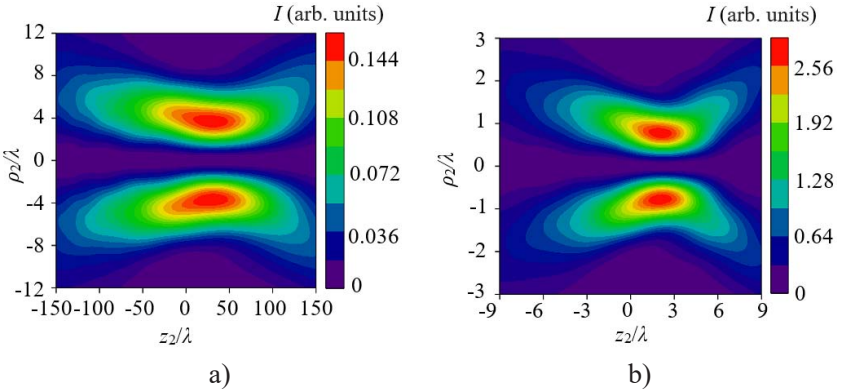


**Figure 4.7. Calculated distributions of the total intensity of the  $TE_{01}+EH_{21}$  mode field at moderate (a) and at sharp (b) focusing in the focal region of the lens**

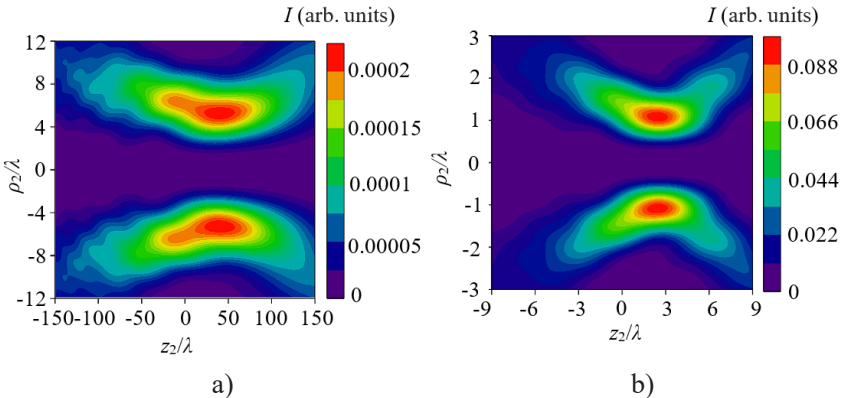


**Figure 4.8. Calculated intensity distributions of the longitudinal component of the  $TE_{01}+EH_{21}$  mode field at moderate (a) and at sharp (b) focusing in the focal region of the lens**

The influence of the numerical aperture  $NA$  of the lens at its different values on the contribution of the longitudinal component of the field to the total intensity of the modes in the focal region of the lens was also calculated according to the formula:

$$\eta(z_2) = \frac{\int_0^{2\pi} \int_0^\infty |E_z(\rho_2, \theta_2, z_2)|^2 \rho_2 d\rho_2 d\theta_2}{\int_0^{2\pi} \int_0^\infty \left[ |E_r(\rho_2, \theta_2, z_2)|^2 + |E_\phi(\rho_2, \theta_2, z_2)|^2 + |E_z(\rho_2, \theta_2, z_2)|^2 \right] \rho_2 d\rho_2 d\theta_2}. \quad (4.11)$$

The calculation results are shown in Figure 4.9 (a). It can be seen that as the numerical aperture of the lens increases, the contribution of the longitudinal component of the field to the total intensity increases. For the  $TM_{01}$ -mode, with the lens numerical aperture of 0.68 specified in the calculations, the contribution of the longitudinal component to the total intensity reaches 20 %, and for the  $EH_{11}$  and  $TE_{01} + EH_{21}$  modes, with the same value of the numerical aperture, it reaches approximately 3 %.

The contribution of the longitudinal field component at sharp focusing ( $F = 36.36$  mm) to the total intensity of  $TM_{01}$ ,  $EH_{11}$ , and  $TE_{01} + EH_{21}$  modes depending on the distance  $z_2$  was also calculated. The calculation results are shown in Fig. 4.9 (b). It can be seen that the growth is observed in a small local area near the focal length of the lens.

### 4.1.3. Comparison of Experimental and Numerical Results

The terahertz laser was used for generation of radiation with nonuniform spatial polarization. Nonuniform mirrors were introduced in the resonator of this laser. The structure of these mirrors is large-scale metallic diffraction gratings with different reflecting periods (Chapter 2). Experimental studies were carried out on a universal setup based on a terahertz laser with optical pumping (Figure 2.10), which allows to study the energy and polarization characteristics of focused laser beams of continuous radiation. For experimental studies, a radiation wavelength of 432.6  $\mu\text{m}$  was chosen (the generation line of a terahertz laser on the molecule of formic acid  $\text{HCOOH}$ , the generation line of a  $\text{CO}_2$  laser with a wavelength of 9.27  $\mu\text{m}$ ). Long-focus (with numerical aperture  $NA = 0.16$ ) and short-focus (with numerical aperture  $NA = 0.68$ ) lenses were used in studying the physical features of focusing terahertz laser beams. These lenses were made from crystalline quartz. In quartz lenses, the  $z$  axis was directed along the optical axis.

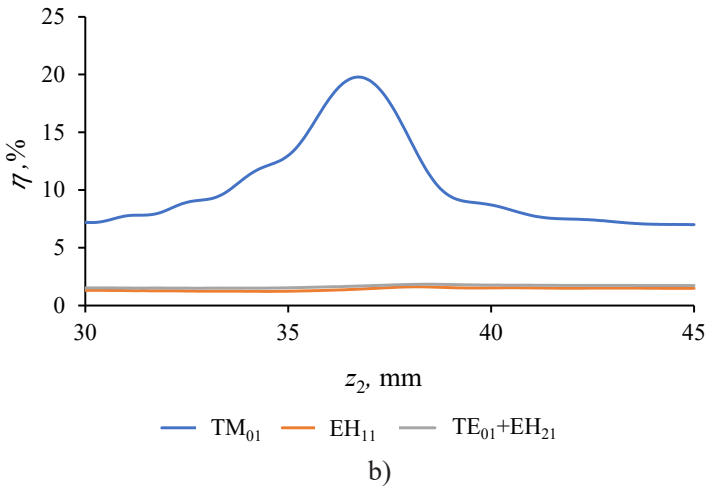
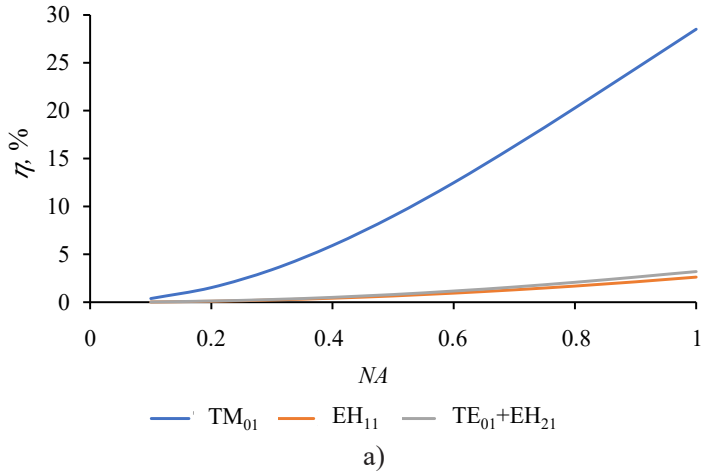


**Figure 4.9. Dependencies of the relative contribution of the longitudinal field components of the  $TM_{01}$ ,  $EH_{11}$ , and  $TE_{01}+EH_{21}$  modes to their total intensity at different values of the numerical aperture of the  $NA$  lens (a) and on the distance  $z_2$  in the focal region during sharp focusing (b)**

*Focusing of linearly polarized radiation.* Mirror I was used in study the physical features of moderate and sharp focusing of linearly polarized terahertz radiation in the resonator of a THz laser (Figure 2.16). The laser was tuned to the spectral line of the linearly polarized symmetric  $\text{EH}_{11}$  mode (Figure 2.27). The normalized transverse distribution of field intensity for this mode at a distance of 300 mm from the output mirror of the laser (in the plane of the lens location) is shown in Figure 4.10. The figure shows a good agreement between experimental and calculated (according to expression 4.9) results.

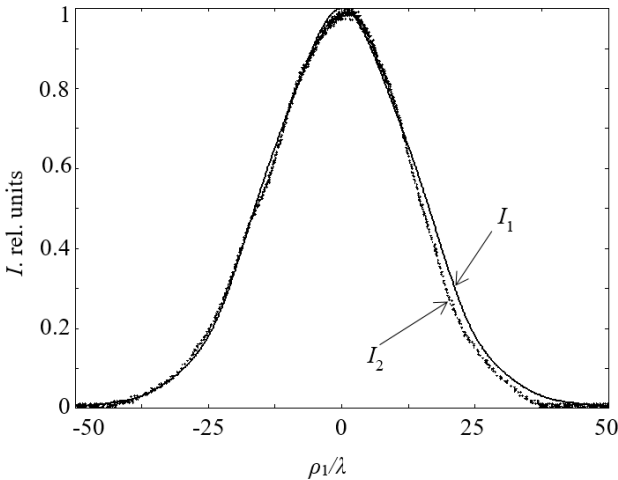


**Figure 4.10. Calculated ( $I_1$ ) and experimental ( $I_2$ ) transverse distributions of the field intensity of the  $\text{EH}_{11}$  mode at a distance of 300 mm from the laser output mirror**

A long-focus lens with a focal length of 160 mm and a short-focus lens with a focal length of 36.36 mm were installed at a distance  $z_2$  from the lens for complete beam interception. By moving the detector 19 (Figure 2.10) along the optical axis in the focal regions of the lenses, the transverse dimensions of the radiation beam of the studied mode FWHM were measured at moderate and at sharp focusing. The results of measurements and numerical calculations are shown in Figures 4.11 – 4.12.

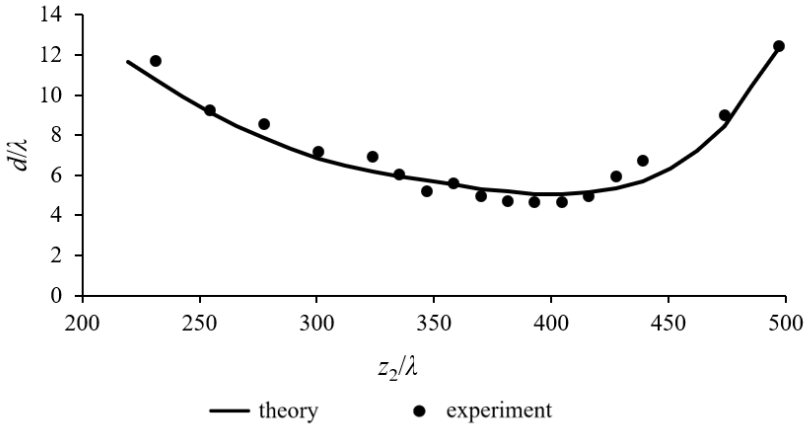


Figure 4.11. Dependence of the beam diameter  $d$  of a moderately focused  $\text{EH}_{11}$  mode on the distance  $z_2$  in the focal region of the lens

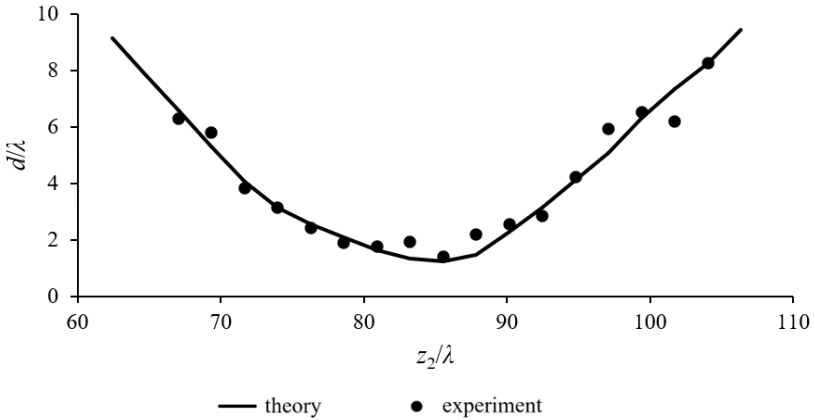


Figure 4.12. Dependence of the beam diameter  $d$  of the sharply focused  $\text{EH}_{11}$  mode on the distance  $z_2$  in the focal region of the lens

The transverse size of the beams  $d$  and the longitudinal distance  $z_2$  are given relative to the radiation wavelength  $\lambda$ . The figures show the coincidence of experimental and calculated data. The minimum diameter of

the focused  $\text{EH}_{11}$  mode at moderate focusing ( $NA = 0.16$ ) in the experiment was  $\text{FWHM} = 4.7 \lambda$  ( $\text{FWHM} = 5.1 \lambda$  – in theory), and at sharp ( $NA = 0.68$ ) in the experiment was  $\text{FWHM} = 1.4 \lambda$  ( $\text{FWHM} = 1.2 \lambda$  – in theory).

The longitudinal size of the focal spot of the focused  $\text{EH}_{11}$  mode was also calculated. The parameter  $l_z$  was defined as the distance at which the diameter of the beam increased by 2 times from its minimum size. At moderate focusing of the  $\text{EH}_{11}$  mode,  $l_z$  it was  $185 \lambda$  in the experiment and it was  $174 \lambda$  in the calculations. At sharp focusing in the experiment, this parameter was equal to  $6.5 \lambda$ , while in theory it was  $6.1 \lambda$ .

Transverse distributions of the intensity of the focused  $\text{EH}_{11}$  mode at moderate and sharp focusing in the focus of the lens are shown in Figures 4.13 – 4.14, respectively. It can be seen from these figures that the transverse distribution of the total field intensity of the linearly polarized  $\text{EH}_{11}$  mode in the region of the minimum size of the focused radiation beams preserves the field maximum, both at moderate and at sharp focusing. Some discrepancy is due to the use of receiver 19 (Figure 2.10) with a spatial resolution of  $0.2 \text{ mm}$  and the aberration of the used lens.

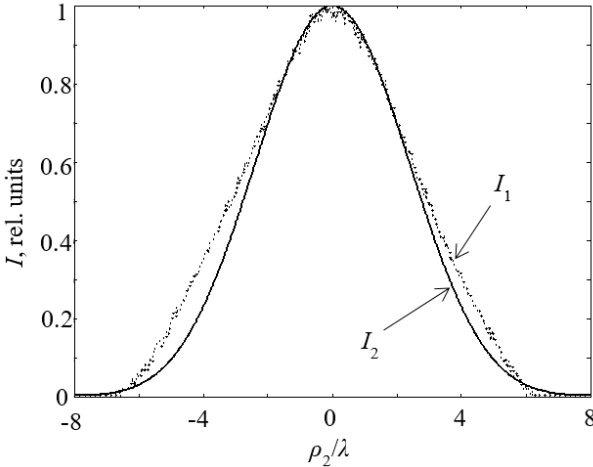


**Figure 4.13. Calculated ( $I_1$ ) and experimental ( $I_2$ ) transverse distributions of the total field intensity of the  $\text{EH}_{11}$  mode at moderate focusing in the focus of the lens**

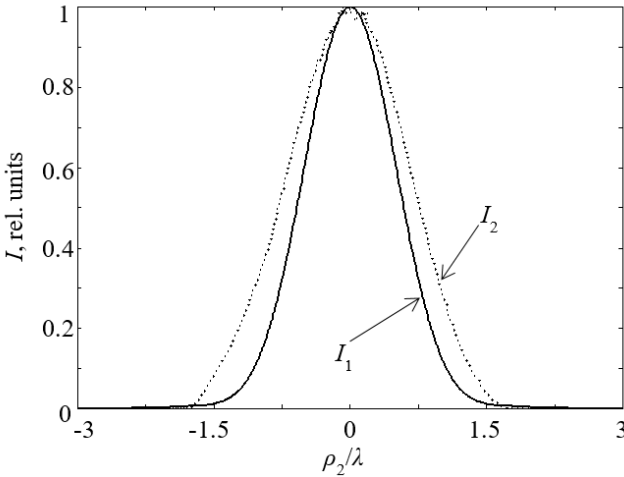


**Figure 4.14. Calculated ( $I_1$ ) and experimental ( $I_2$ ) transverse distributions of the total intensity of the  $\text{EH}_{11}$  mode field at sharp focusing in the focus of the lens**

*Focusing of azimuthally polarized radiation.* Large-scale input and output homogeneous mirrors were used for study the focusing of azimuthally polarized terahertz radiation which is formed in the resonator of a THz laser. (Figure 2.13). The laser was tuned to the spectral line of the azimuthally polarized symmetric  $\text{TE}_{01}$  mode (Figure 2.14). The distribution of the field intensity of this mode in a cross-section at a distance of 300 mm from the output mirror of the laser (in the plane of the location of the lens) is shown in Figure 4.15. The figure shows a good agreement between experimental and calculated (according to expression 4.8) results.

By moving the detector 19 (Figure 2.10) along the optical axis in the focal regions of the lenses, the transverse size FWHM and longitudinal dimensions of the beam of the investigated mode were measured at moderate and sharp focusing. The results of measurements and numerical calculations are shown in Figures 4.16 – 4.17.

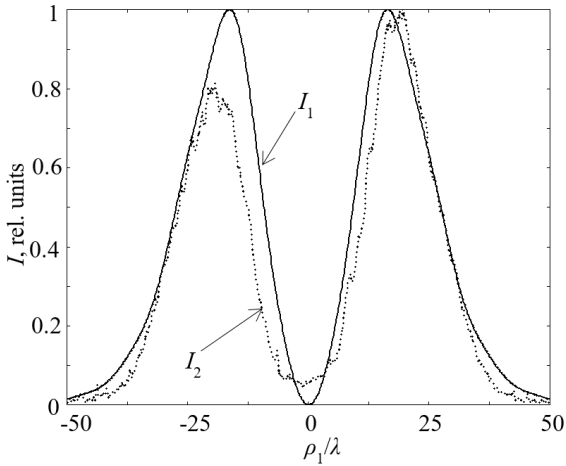


Figure 4.15. Calculated ( $I_1$ ) and experimental ( $I_2$ ) transverse distributions of the  $TE_{01}$  mode field intensity at a distance of 300 mm from the laser output mirror

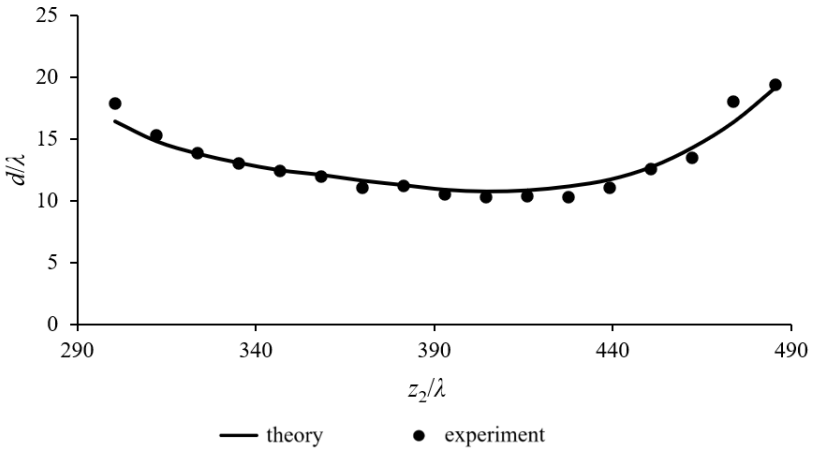
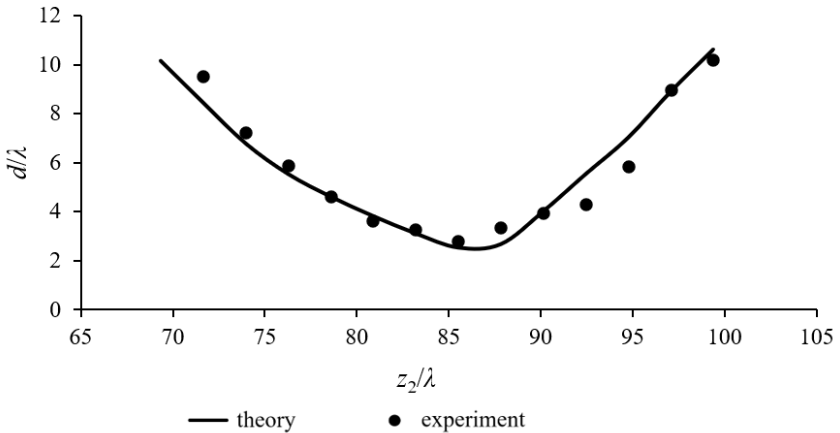


Figure 4.16. Dependence of the beam diameter  $d$  of a moderately focused  $TE_{01}$  mode on the distance  $z_2$  in the focal region of the lens

The figures show a good agreement between the experimental and calculated data. The minimum diameter of the focused  $TE_{01}$  mode at moderate focusing ( $NA = 0.16$ ) in the experiment was  $FWHM = 10.3 \lambda$  ( $FWHM = 10.8 \lambda$  – in theory), and at sharp focusing ( $NA = 0.68$ ) in the experiment was  $FWHM = 2.8 \lambda$  ( $FWHM = 2.5 \lambda$  – in theory). At the same time, the size of the focal spot  $\ell_z$  of the focused  $TE_{01}$  mode at moderate focusing in the experiment was  $144 \lambda$ , and in the calculations it was  $153 \lambda$ . At sharp focusing of this mode, it was  $9.6 \lambda$  in the experiment and it was  $8.3 \lambda$  in theory.



**Figure 4.17. Dependence of the beam diameter  $d$  of the sharply focused  $TE_{01}$  mode on the distance  $z_2$  in the focal region of the lens**

Transverse distributions of the intensity of the focused  $TE_{01}$  mode at moderate and at sharp focusing are shown in Figures 4.18 – 4.19, respectively. It can be seen from the figures that the transverse distribution of the total field intensity of the azimuthally polarized  $TE_{01}$  mode of the dielectric waveguide in the region of the minimum size of the focused radiation beams retains a ring-like appearance both at moderate and at sharp focusing. The experimental and calculated distributions of the focused  $TE_{01}$  mode almost coincide.

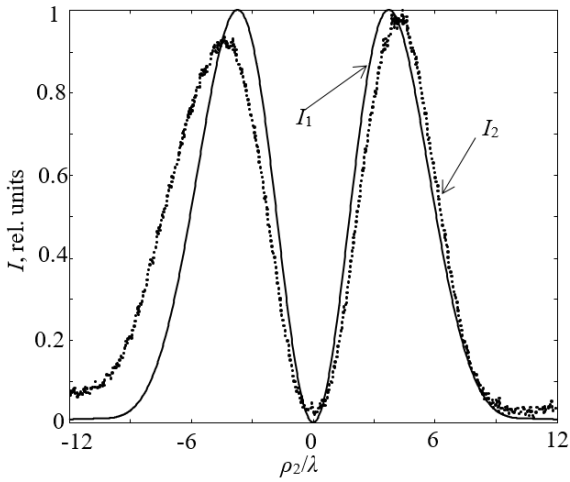


Figure 4.18. Calculated ( $I_1$ ) and experimental ( $I_2$ ) transverse distributions of the total  $TE_{01}$  mode field intensity at moderate focusing in the focus of the lens

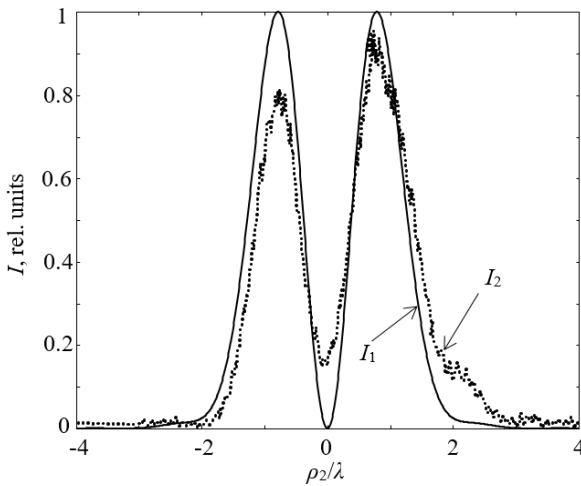
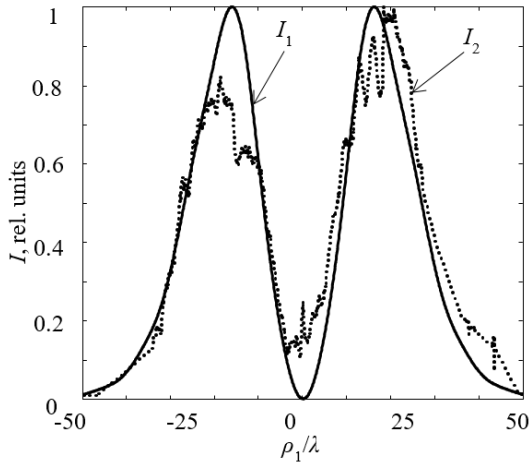


Figure 4.19. Calculated ( $I_1$ ) and experimental ( $I_2$ ) transverse distributions of the total intensity of the  $TE_{01}$  mode field at sharp focusing in the focus of the lens

*Focusing of radially polarized radiation.* A radially symmetric diffraction mirror III with a reflecting center was used for study the focusing of radially polarized laser radiation which is formed in the resonator of a THz laser (Figure 2.22). The laser was tuned to the spectral line of the radially polarized symmetric  $TM_{01}$  mode (Figure 2.29). The distribution of the field intensity of this mode in a cross-section at a distance of 300 mm from the output mirror of the laser (in the plane of the location of the lens) is shown in Figure 4.20. The figure shows a good agreement between experimental and calculated (according to expression 4.7) results.



**Figure 4.20. Calculated ( $I_1$ ) and experimental ( $I_2$ ) transverse distributions of the  $TM_{01}$  mode field intensity at a distance of 300 mm from the laser output mirror**

It can be seen from the figure that the  $TM_{01}$  mode maintains a ring-shaped appearance at the lens placement distance. After alternately placement long-focus and short-focus lenses, the transverse size and longitudinal size of the radiation beam of the investigated mode were measured. The results of the calculations are shown in Figures 4.21 – 4.22, respectively. The figures show a good agreement between the experimental and calculated data. The minimum diameter of the focused  $TM_{01}$  mode at moderate focusing ( $NA = 0.16$ ) in the experiment was  $FWHM = 12.0 \lambda$  ( $FWHM = 11.9 \lambda -$

in theory), and at sharp focusing ( $NA = 0.68$ ) in the experiment was  $FWHM = 2.9 \lambda$  ( $FWHM = 2.7 \lambda$  – in theory).

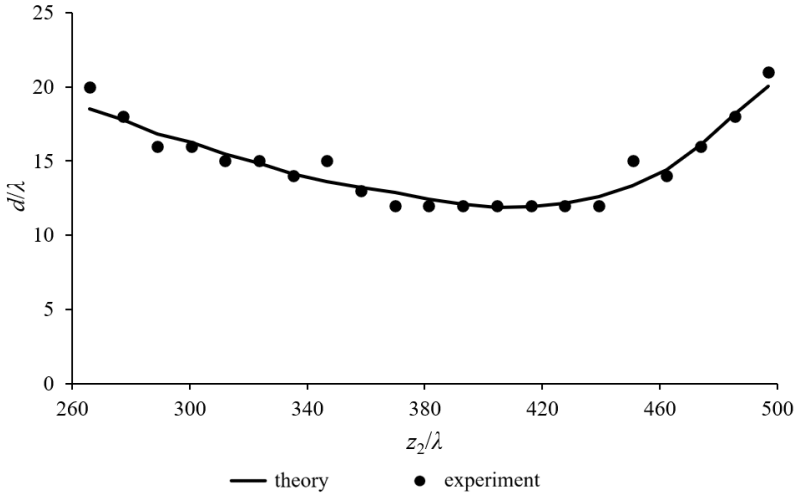


**Figure 4.21. Dependence of the beam diameter  $d$  of a moderately focused  $TM_{01}$  mode on the distance  $z_2$  in the focal region of the lens**

At the same time, the size of the focal spot  $\ell_z$  of the focused  $TM_{01}$  mode at moderate focusing in the experiment was equal to  $233 \lambda$ , and in theoretical calculations was  $215 \lambda$ . At sharp focusing of this mode, it was  $9.8 \lambda$  in the experiment and it was  $9.2 \lambda$  in theory.

Transverse distributions of the intensity of the focused  $TM_{01}$  mode at moderate and at sharp focusing are shown in Figures 4.23 – 4.24, respectively. It can be seen that for the  $TM_{01}$  mode of the dielectric waveguide at sharp focusing, there is a significant increase in the axial intensity in the field distribution both in theory and experiment (Figure 4.24). At the same time, at moderate focusing, the transverse distributions of the  $TM_{01}$  mode retains its annular shape and has a dip on the beam axis (Figure 4.23).

In this regard, the influence of the numerical aperture of the lens on the transverse distribution of the  $TM_{01}$  mode field intensity was calculated. The results of the calculations are presented in Figure 3.25.

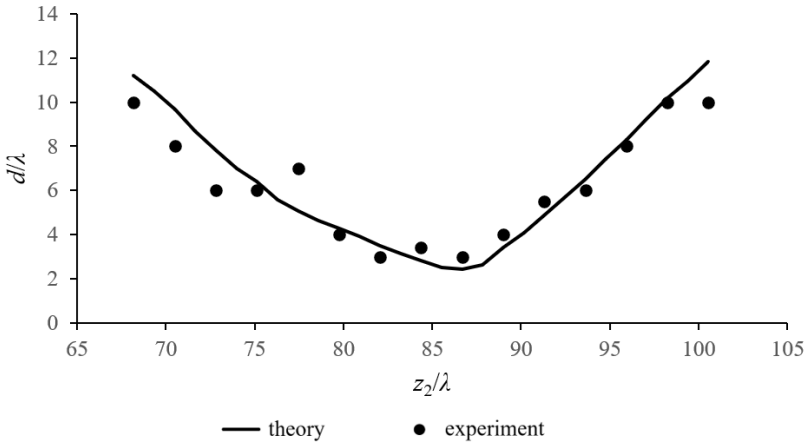


**Figure 4.22.** Dependence of the beam diameter  $d$  of a sharply focused  $TM_{01}$ -mode on the distance  $z_2$  in the focal region of the lens

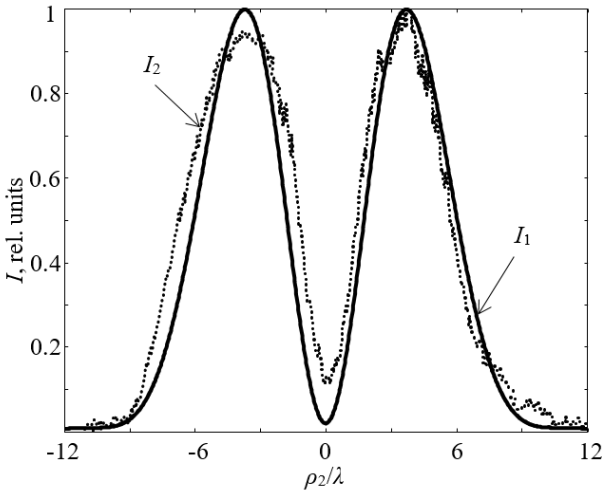


**Figure 4.23.** Calculated ( $I_1$ ) and experimental ( $I_2$ ) transverse distributions of the total  $TM_{01}$  mode field intensity at moderate focusing in the focus of the lens

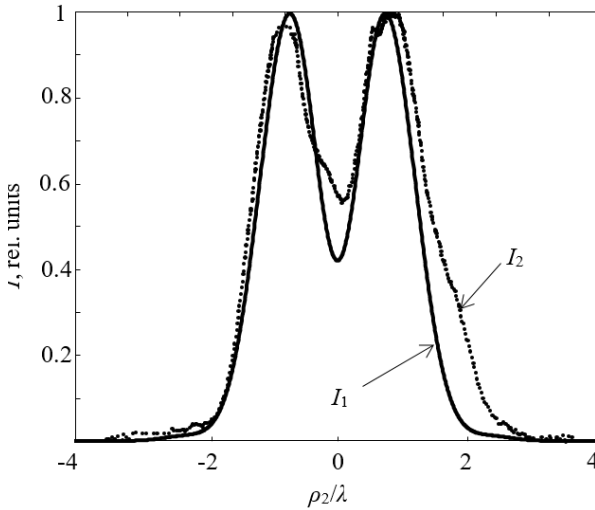


**Figure 4.24. Calculated ( $I_1$ ) and experimental ( $I_2$ ) transverse distributions of the total intensity of the  $TM_{01}$  mode field at sharp focusing in the focus of the lens**

As can be seen from the presented results, with the growth of the numerical aperture of the lens, the axial intensity of this mode field increases. At  $NA \sim 1$ , its distribution completely loses its ring-like shape and acquires maximum intensity on the axis.

Theoretical and experimental data of minimum diameters of focal spots of focused modes and their longitudinal dimensions are given in Table 4.1.

Table 4.1

**Minimum diameters and longitudinal dimensions of focal spots of focused modes**

Mod types	$NA = 0.68$				$NA = 0.16$			
	FWHM		$\ell_z$		FWHM		$\ell_z$	
	Theor.	Exper.	Theor.	Exper.	Theor.	Exper.	Theor.	Exper.
$TE_{01}$	$2.5 \lambda$	$2.8 \lambda$	$8.3 \lambda$	$9.6 \lambda$	$10.8 \lambda$	$10.3 \lambda$	$153 \lambda$	$144 \lambda$
$TM_{01}$	$2.7 \lambda$	$2.9 \lambda$	$9.2 \lambda$	$9.8 \lambda$	$11.9 \lambda$	$12.0 \lambda$	$215 \lambda$	$233 \lambda$
$EH_{11}$	$1.2 \lambda$	$1.4 \lambda$	$6.1 \lambda$	$6.5 \lambda$	$5.1 \lambda$	$4.7 \lambda$	$174 \lambda$	$185 \lambda$

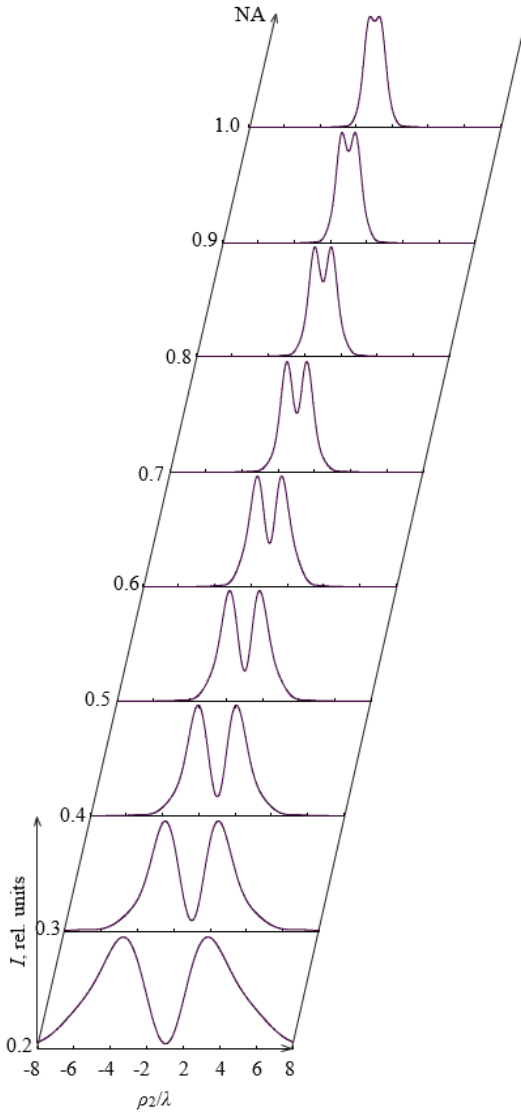


**Figure 4.25. Dynamics of changes in the transverse distribution of the  $TM_{01}$ -mode depending on the numerical aperture of the lens**

## 4.2. FOCUSING OF HIGHER-ORDER MODES

### 4.2.1. Theoretical Relations

In the initial plane (on the output mirror of the laser), we set the radiation in the form of higher ( $n > 1$ ) azimuthally, radially and linearly polarized  $TE_{0n}$ ,  $TM_{0n}$ ,  $EH_{1n}$  modes of a circular hollow dielectric waveguide of radius  $a_1$  (Figure 4.1). The field components for these modes in the source plane in the cylindrical coordinate system are described by the expressions:

$$TE_{0n} \text{ mode: } \begin{cases} \vec{E}_r(r, \phi) = 0, \\ \vec{E}_\phi(r, \phi) = A_{0n} \frac{\chi_{0n}}{a_1} J_1\left(\chi_{0n} \frac{r}{a_1}\right), \end{cases} \quad (4.12)$$

$$TM_{0n} \text{ mode: } \begin{cases} \vec{E}_r(r, \phi) = B_{0n} \frac{1}{a_1} J_1\left(\chi_{0n} \frac{r}{a_1}\right), \\ \vec{E}_\phi(r, \phi) = 0, \end{cases} \quad (4.13)$$

$$EH_{1n} \text{ mode: } \begin{cases} \vec{E}_r(r, \phi) = C_{1n} J_0\left(\chi_{1n} \frac{r}{a_1}\right) \sin(\phi), \\ \vec{E}_\phi(r, \phi) = C_{1n} J_0\left(\chi_{1n} \frac{r}{a_1}\right) \cos(\phi), \end{cases} \quad (4.14)$$

where  $A_{0n} = \frac{1}{\sqrt{\pi} \chi_{0n} J_0(\chi_{0n})}$ ,  $B_{0n} = \frac{1}{\sqrt{\pi} J_2(\chi_{1n})}$ ,  $C_{11} = \frac{1}{a \sqrt{\pi} J_1(\chi_{1n})}$  are

the normalizing factors;  $J_0, J_1, J_2$  are the Bessel functions of the first order;  $\chi_{0n}, \chi_{1n}$  are the roots of the equation  $J_1(\chi) = 0$ .

Using the Rayleigh-Sommerfeld vector theory [142] in the nonparaxial approximation and expressions (4.12–4.14), we find the field components  $TE_{0n}$ ,  $TM_{0n}$ ,  $EH_{1n}$  modes of the dielectric waveguide resonator in free space at a distance  $z_1$ . After multiplying the obtained expressions by the lens phase correction function [148] and again applying the Rayleigh-Sommerfeld integrals to them, we write down the components of the data mode field in the focal region of the lens.

Field components for azimuthally polarized  $TE_{0n}$  modes at a distance  $z_2$  from the lens have the form:

$$\left\{ \begin{array}{l} E_r(\rho_2, \theta_2, z_2) = 0, \\ E_\phi(\rho_2, \theta_2, z_2) = -\frac{k^2 z_1 z_2}{\xi_2^2} \exp(ik\xi_2) A_{0n} \int_0^{a_2} \frac{\exp(ik\xi_1)}{\xi_1^2} \int_0^{a_1} J_1\left(\chi_{0n} \frac{r}{a_1}\right) \times \\ \quad \times J_1(\gamma_1 r) \exp\left(\frac{ikr^2}{2\xi_1}\right) r dr J_1(\gamma_2 \rho_1) \exp\left(\frac{ik\rho_1^2}{2\xi_2}\right) Ph(\rho_1) \rho_1 d\rho_1, \\ E_z(\rho_2, \theta_2, z_2) = 0. \end{array} \right. \quad (4.15)$$

Field components for linearly polarized  $EH_{1n}$  modes at a distance  $z_2$  from the lens have the form:

$$\left\{ \begin{array}{l} E_r(\rho_2, \theta_2, z_2) = \frac{k^2 z_1 z_2}{\xi_2^2} \exp(ik\xi_2) \sin(\theta_2) C_{1n} \int_0^{a_2} \frac{\exp(ik\xi_1)}{\xi_1^2} \times \int_0^{a_1} J_0\left(\chi_{0n} \frac{r}{a_1}\right) \times \\ \quad \times J_0(\gamma_1 r) \exp\left(\frac{ikr^2}{2\xi_1}\right) r dr J_0(\gamma_2 \rho_1) \exp\left(\frac{ik\rho_1^2}{2\xi_2}\right) Ph(\rho_1) \rho_1 d\rho_1, \\ E_\phi(\rho_2, \theta_2, z_2) = \frac{k^2 z_1 z_2}{\xi_2^2} \exp(ik\xi_2) \cos(\theta_2) C_{1n} \int_0^{a_2} \frac{\exp(ik\xi_1)}{\xi_1^2} \int_0^{a_1} J_0\left(\chi_{0n} \frac{r}{a_1}\right) \times \\ \quad \times J_0(\gamma_1 r) \exp\left(\frac{ikr^2}{2\xi_1}\right) r dr J_0(\gamma_2 \rho_1) \exp\left(\frac{ik\rho_1^2}{2\xi_2}\right) Ph(\rho_1) \rho_1 d\rho_1, \\ E_z(\rho_2, \theta_2, z_2) = \frac{ik^2 z_1}{\xi_2^2} \exp(ik\xi_2) \sin(\theta_2) C_{1n} \int_0^{a_2} \frac{\exp(ik\xi_1)}{\xi_1^2} \int_0^{a_1} J_0\left(\chi_{0n} \frac{r}{a_1}\right) \times \\ \quad \times J_0(\gamma_1 r) \exp\left(\frac{ikr^2}{2\xi_1}\right) r dr \times [i\rho_1 J_1(\gamma_2 \rho_1) + \rho_2 J_1(\gamma_2 \rho_1)] \times \\ \quad \times \exp\left(\frac{ik\rho_1^2}{2\xi_2}\right) Ph(\rho_1) \rho_1 d\rho_1. \end{array} \right. \quad (4.16)$$

Field components for radially polarized  $TM_{0n}$  modes at a distance  $z_2$  from the lens have the form:

$$\left\{ \begin{aligned}
 E_r(\rho_2, \theta_2, z_2) &= \frac{k^2 z_1 z_2}{\xi_2^2} \exp(ik\xi_2) B_{0n} \int_0^{a_2} \frac{\exp(ik\xi_1)}{\xi_1^2} \int_0^{a_1} J_1\left(\chi_{0n} \frac{r}{a_1}\right) J_1(\gamma_1 r) \times \\
 &\quad \times \exp\left(\frac{ikr^2}{2\xi_1}\right) r dr J_1(\gamma_2 \rho_1) \exp\left(\frac{ik\rho_1^2}{2\xi_2}\right) Ph(\rho_1) \rho_1 d\rho_1, \\
 E_\phi(\rho_2, \theta_2, z_2) &= 0, \\
 E_z(\rho_2, \theta_2, z_2) &= \frac{ik^2 z_1}{\xi_2^2} \exp(ik\xi_2) B_{0n} \int_0^{a_2} \frac{\exp(ik\xi_1)}{\xi_1^2} \int_0^{a_1} J_1\left(\chi_{0n} \frac{r}{a_1}\right) J_1(\gamma_1 r) \times \\
 &\quad \times \exp\left(\frac{ikr^2}{2\xi_1}\right) r dr [\rho_1 J_0(\gamma_2 \rho_1) + i\rho_2 J_1(\gamma_2 \rho_1)] \exp\left(\frac{ik\rho_1^2}{2\xi_2}\right) Ph(\rho_1) \rho_1 d\rho_1.
 \end{aligned} \right. \quad (4.17)$$

#### 4.2.2. Calculation Results and Their Analysis

Using expressions 4.15 – 4.17, the total field intensity of  $TE_{0n}$ ,  $TM_{0n}$ ,  $EH_{1n}$  modes  $I(\rho_2, \theta_2, z_2) = |E_r|^2 + |E_\phi|^2 + |E_z|^2$  was studied, as well as the intensity of the longitudinal component of  $TM_{0n}$  modes in the region of the minimum size of the focused beam at sharp and at moderate focusing.

Figures 4.26 – 4.27 show the distributions of the total field intensity of linearly polarized  $EH_{12}$  and  $EH_{13}$  modes at moderate and at sharp focusing. On the axis, the total field intensity of the given modes, which is determined by all three components, has a maximum. The maximum intensity of the field for the  $EH_{1n}$  mode at moderate focusing is at the distance  $z_{I_{max}} = 75.13 \lambda$ , at sharp focusing –  $z_{I_{max}} = 4.71 \lambda$ .

Due to the complex structure of the field of higher-order modes, their diameter  $d_\sigma$  was calculated according to the formula [149]:

$$d_\sigma = 2 \sqrt{\frac{2 \int_0^{2\pi} \int_0^\infty \rho_2^2 I(\rho_2, \theta_2, z_2) \rho_2 d\rho_2 d\theta_2}{\int_0^{2\pi} \int_0^\infty I(\rho_2, \theta_2, z_2) \rho_2 d\rho_2 d\theta_2}}. \quad (4.18)$$

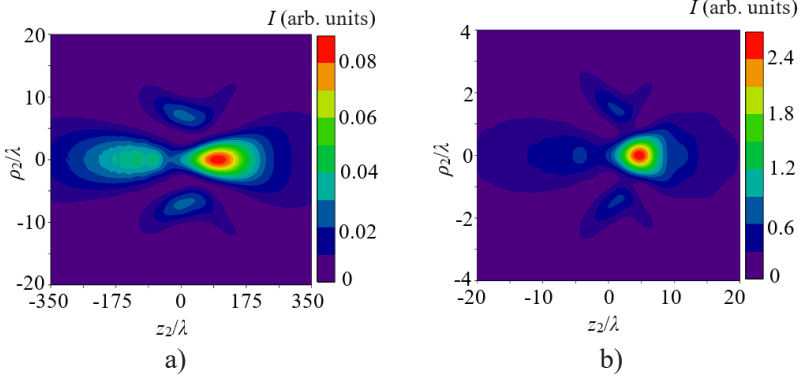


**Figure 4.26.** Calculated distributions of the total intensity of the  $\text{EH}_{12}$  mode field at moderate (a) and at sharp (b) focusing in the focal region of the lens

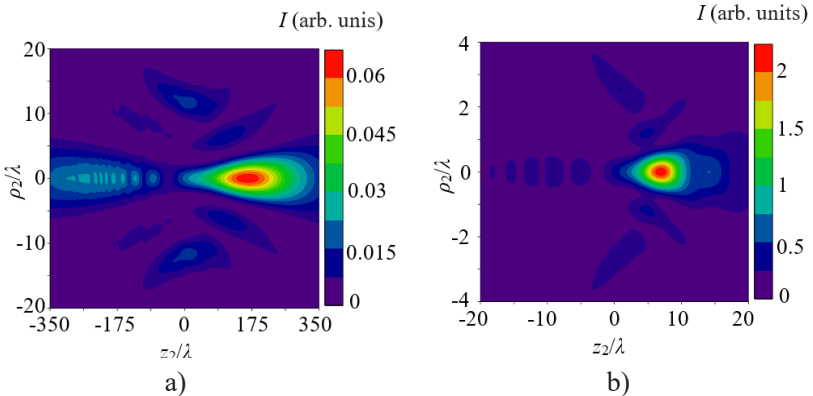


**Figure 4.27.** Calculated distributions of the total intensity of the  $\text{EH}_{13}$  mode field at moderate (a) and at sharp (b) focusing in the focal region of the lens

Using this expression, it was found that the diameter of the  $\text{EH}_{12}$  mode beam in the region of maximum field intensity at moderate focusing is equal to  $d_{\sigma} = 26.49\lambda$ , and at sharp focusing is  $d_{\sigma} = 6.22\lambda$ .

The maximum intensity of the  $\text{EH}_{13}$  mode field at moderate focusing is at the distance  $z_{\text{Imax}} = 139.85\lambda$ , and at sharp focusing is  $z_{\text{Imax}} = 6.80\lambda$

(Figure 4.27). At the same time, the diameter of the beam in this area at moderate focusing for the  $EH_{13}$  mode was  $d_{\sigma} = 42.99\lambda$ , and at sharp focusing was  $d_{\sigma} = 10.34\lambda$ .

Figures 4.28 – 4.29 show the distribution of the total field intensity of azimuthally polarized  $TE_{02}$  and  $TE_{03}$  modes at moderate and at sharp focusing.

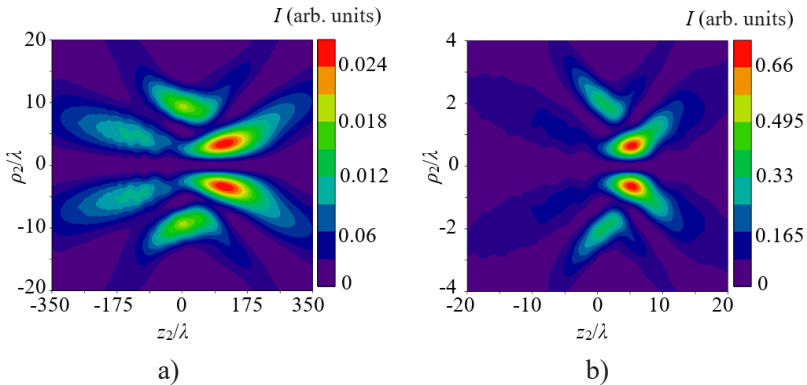


**Figure 4.28. Calculated distributions of the total intensity of the  $TE_{02}$  mode field at moderate (a) and at sharp (b) focusing in the focal region of the lens**

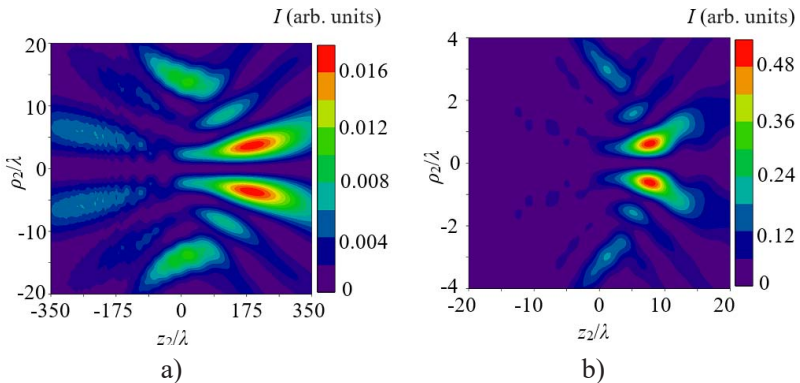


**Figure 4.29. Calculated distributions of the total intensity of the  $TE_{03}$ -mode field at moderate (a) and at sharp (b) focusing in the focal region of the lens**

The transverse distribution of the total field intensity of the azimuthally polarized  $TE_{02}$  and  $TE_{03}$  modes of the dielectric waveguide resonator in the focal region retains a ring-like appearance (Figures 4.28 – 4.29) both at moderate and at sharp focusing. The field maximum has the central lobes of these modes, which are noticeably shifted from the focus of the lens. The maximum field intensity for the  $TE_{02}$  mode at moderate focusing is at the distance  $z_{Imax} = 98.24 \lambda$ , and at sharp focusing is  $z_{Imax} = 4.95 \lambda$ . The diameter of the beam in this region at moderate focusing for the  $TE_{02}$  mode was  $d_{\sigma} = 34.10\lambda$ , and at sharp focusing was  $d_{\sigma} = 8.14\lambda$ . For the  $TE_{03}$  mode, the maximum field intensity at moderate focusing is at the distance  $z_{Imax} = 164.12 \lambda$ , and at sharp focusing is  $z_{Imax} = 7.95 \lambda$  (Figure 4.29). At the same time, the diameter of the beam in the region of maximum intensity for this mode was  $d_{\sigma} = 51.95\lambda$  at moderate and was  $d_{\sigma} = 7.95\lambda$  at sharp focusing. In addition, the total intensity for both modes were determined by only one transverse component (4.15).

Distributions of the total field intensity of radially polarized  $TM_{02}$  and  $TM_{03}$  modes at moderate and at sharp focusing are shown in Figures 4.30 – 4.31. It can be seen from the graphs that at sharp focusing, an increase in axial intensity is observed in the transverse distribution of the data mode field (Figure 4.30 b, Figure 4.31 b), which is absent at moderate focusing (Figure 4.30 a, Figure 4.31 a).

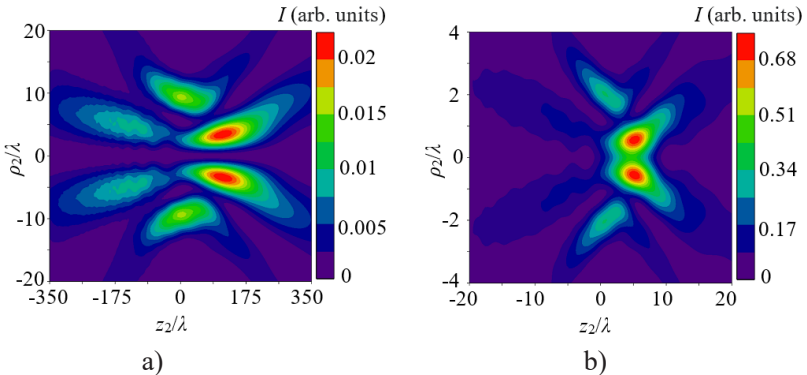


**Figure 4.30.** Calculated distributions of the total intensity of the  $TM_{02}$  mode field at moderate (a) and at sharp (b) focusing in the focal region of the lens

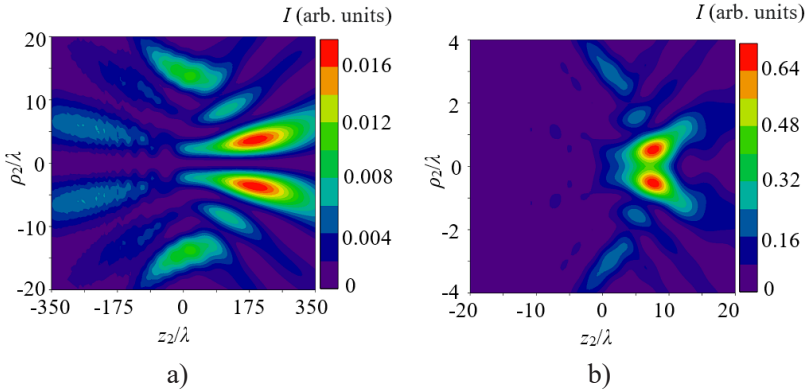


**Figure 4.31. Calculated distributions of the total intensity of the  $TM_{03}$  mode field at moderate (a) and at sharp (b) focusing in the focal region of the lens**

The maximum intensity of the  $TM_{02}$  mode field at moderate focusing is at the distance  $z_{lmax} = 90.15 \lambda$ , and at sharp focusing is  $z_{lmax} = 5.18 \lambda$  (Figure 3.30). The diameter of the beam in this region at moderate focusing for the  $TM_{02}$  mode was  $d_{\sigma} = 34.48\lambda$ , and at sharp focusing was  $d_{\sigma} = 10.55\lambda$ .

In the  $TM_{03}$  mode, the maximum field intensity at moderate focusing is at the distance  $z_{lmax} = 153.72 \lambda$ , and at sharp focusing is  $7.25 \lambda$  (Figure 4.31). At the same time, the diameter of the beam in the region of maximum intensity for this mode was  $d_{\sigma} = 53.17\lambda$  at moderate and it was  $d_{\sigma} = 7.25\lambda$  at sharp focusing. It is also worth noting that the total field intensity for these modes was determined by two components  $E_r$  and  $E_z$ .

The longitudinal component of the  $TM_{02}$  and  $TM_{03}$  mode field during sharp focusing makes a significant contribution to the total intensity of these modes (Figure 4.32 b, Figure 4.33 b).

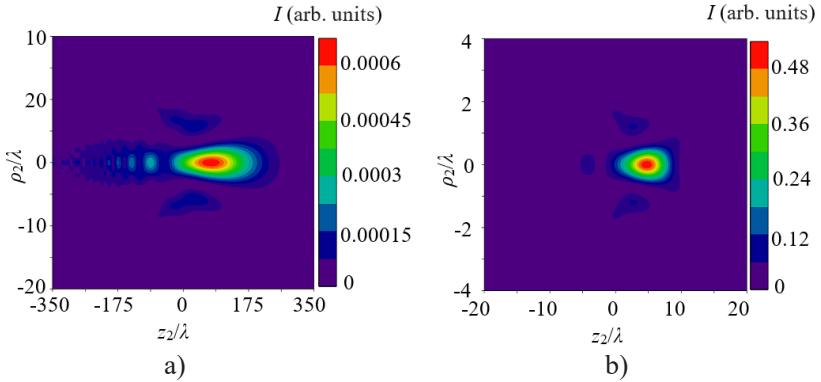


**Figure 4.32.** Calculated distributions of the intensity of the longitudinal component of the  $TM_{02}$  mode field at moderate (a) and at sharp (b) focusing in the focal region of the lens

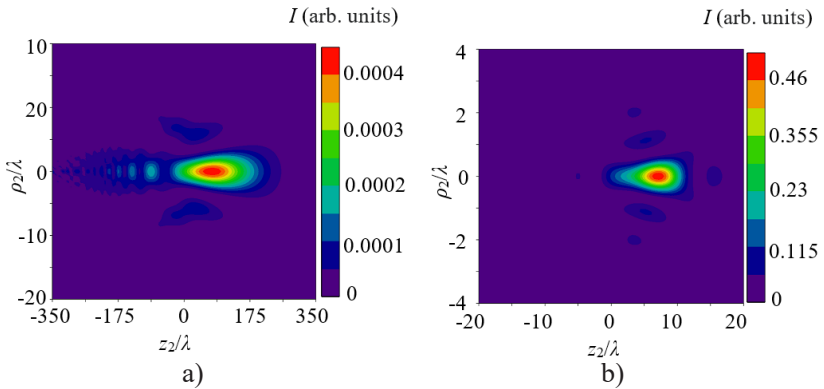


**Figure 4.33.** Calculated distributions of the intensity of the longitudinal component of the  $TM_{03}$  mode field at moderate (a) and at sharp (b) focusing in the focal region of the lens

### 4.2.3. Comparison of Experimental and Numerical Results

An output homogeneous and an input inhomogeneous phase-stepped mirrors were used to study the focusing of higher-order modes in the THz laser resonator (Figure 2.34). The laser was tuned to the spectral line of

the linearly polarized higher mode  $\text{EH}_{12}$  (Figure 2.35). The calculated and experimental distributions of the field intensity of this mode in the cross-section at a distance of 300 mm from the output mirror of the laser (in the plane of the location of the lens) are shown in Figures 4.34 – 4.35.

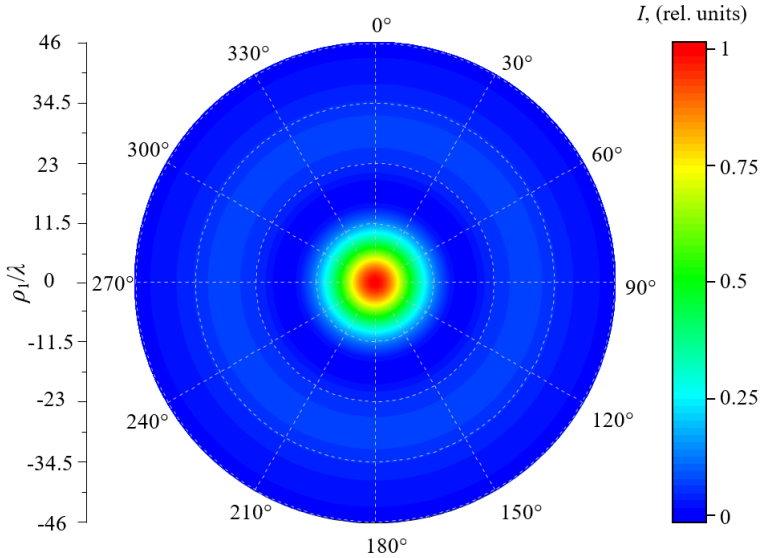


**Figure 4.34. Calculated transverse distribution of the  $\text{EH}_{12}$  mode field intensity at a distance of 300 mm from the laser output mirror**

The beam diameter of this mode in free space in the experiment was  $\text{FWHM} = 16.5 \lambda$ , and in theory was  $\text{FWHM} = 15.96 \lambda$ . The figures also show the coincidence of the shape of the  $\text{EH}_{12}$  mode in the experimental and calculated results.

A long-focus lens with a focal length of 160 mm and a short-focus lens with a focal length of 36.36 mm were placed at a distance of  $z = 300$  mm for completely intercept the beam. By moving the detector 19 (Figure 2.10) along the optical axis in the focal regions of the lenses, the transverse size of the radiation beam of the studied mode was measured at moderate and at sharp focusing.

It was experimentally found that the maximum field intensity of the  $\text{EH}_{12}$  mode at moderate focusing is at the distance  $z_{lmax} = 74.80 \lambda$ , in calculations is  $z_{lmax} = 75.13 \lambda$ . At sharp focusing in the experiment, the maximum field intensity of this mode was at the distance  $z_{lmax} = 4.6 \lambda$ , in theory  $z_{lmax} = 4.71 \lambda$ .

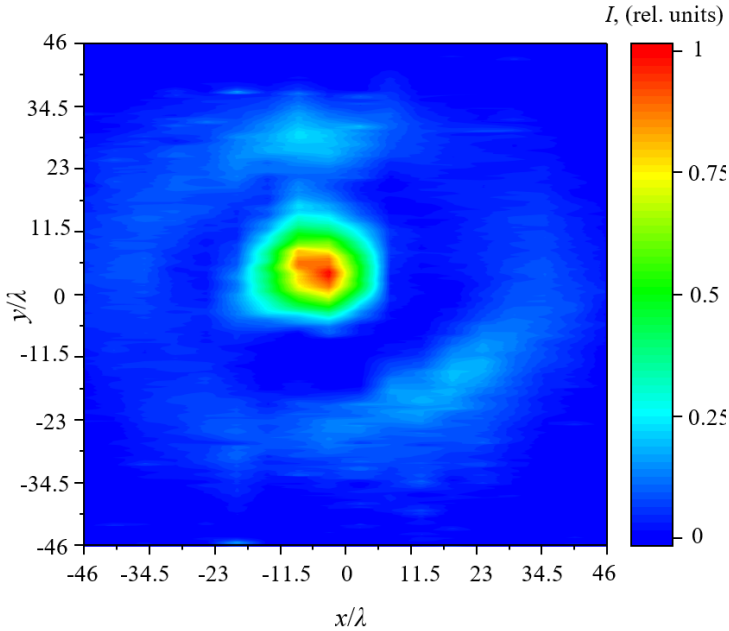


**Figure 4.35. Experimental transverse distribution of the  $\text{EH}_{12}$  mode field intensity at a distance of 300 mm from the laser output mirror**

Transverse intensity distributions at the obtained distances of the focused  $\text{EH}_{12}$  mode at moderate and at sharp focusing are shown in Figures 4.36 – 4.37.

The diameter of the focused  $\text{EH}_{12}$  mode at moderate focusing ( $NA = 0.16$ ) in the experiment was  $\text{FWHM} = 4.50 \lambda$  ( $\text{FWHM} = 4.48 \lambda$  – in theory), and at sharp focusing ( $NA = 0.68$ ) in the experiment was  $\text{FWHM} = 0.90 \lambda$  ( $\text{FWHM} = 1.27 \lambda$  – in theory).

The theoretical results of the location of the positions of the maximum field intensity of the higher-order modes from the  $z_{lmax}$  focus, as well as their diameters in this area are given in Table 4.2.

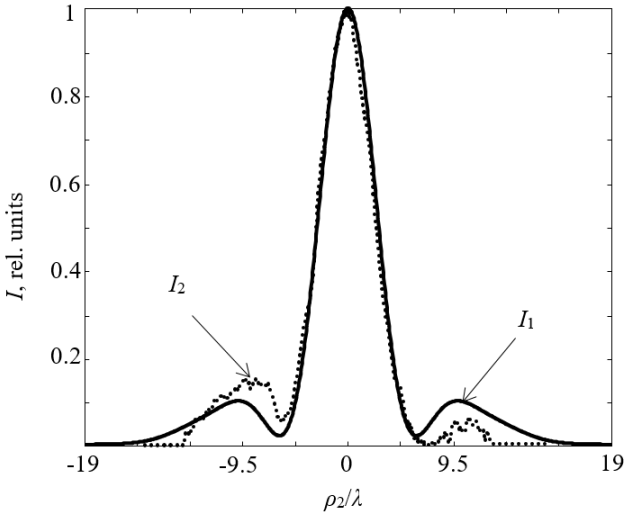


**Figure 4.36. Calculated ( $I_1$ ) and experimental ( $I_2$ ) transverse distributions of the total field intensity of the  $EH_{11}$  mode at moderate focusing**

Table 4.2

**The results of finding positions of maximum intensity higher-order modes and the diameters of their focal spots**

Mod types	$NA = 0.68$		$NA = 0.16$	
	$z_{lmax}/\lambda$	$d_{\sigma}/\lambda$	$z_{lmax}/\lambda$	$d_{\sigma}/\lambda$
$EH_{12}$	4.71	6.22	75.13	26.50
$EH_{13}$	6.80	10.34	139.85	42.99
$TE_{02}$	4.95	8.14	98.24	34.10
$TE_{03}$	7.95	13.11	164.12	51.95
$TM_{02}$	5.18	10.55	90.15	34.48
$TM_{03}$	7.26	17.72	153.72	53.17

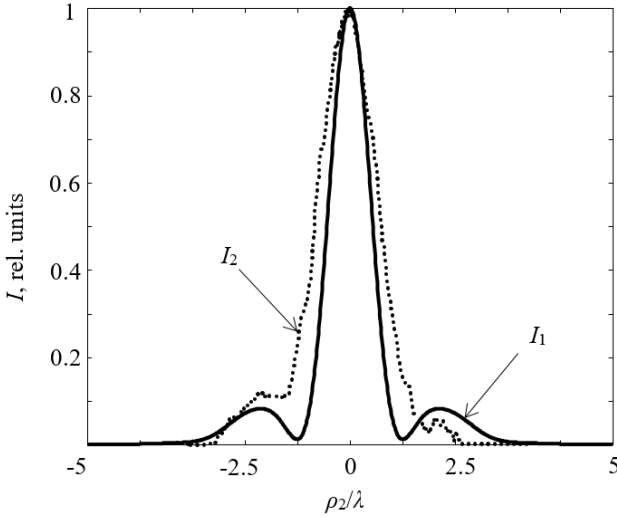


**Figure 4.37. Calculated ( $I_1$ ) and experimental ( $I_2$ ) transverse distributions of the total field intensity of the  $\text{EH}_{12}$  mode at moderate focusing**

### 4.3. FOCUSING OF RADIATION OF TERAHERTZ LASER BASED ON A METALLIC CIRCULAR WAVEGUIDE

#### 4.3.1. Theoretical Relations

The modes of the studied laser resonator coincide with the modes of a circular metal waveguide. In this regard, let us set radiation in the form of symmetric  $\text{TE}_{0n}$ ,  $\text{TM}_{0n}$  and asymmetric  $\text{TE}_{1n}$ ,  $\text{TM}_{1n}$  modes (Figure 4.38) of a circular metal waveguide of radius  $a$  (Figure 4.39) in the initial plane (at the output mirror of the laser). The normalized components of the electromagnetic field of these modes in the source plane  $z = 0$  have a form [51]:

$$\begin{cases} \vec{E}_r^{\text{TE}_{mn}}(r, \phi) = \pm \bar{r}_0 A_{mn} \frac{m}{r} J_m \left( \chi'_{mn} \frac{r}{a} \right) \begin{cases} \sin(m\phi) \\ \cos(m\phi) \end{cases}, \\ \vec{E}_\phi^{\text{TE}_{mn}}(r, \phi) = \bar{\phi}_0 A_{mn} \frac{\chi'_{mn}}{a} J'_m \left( \chi'_{mn} \frac{r}{a} \right) \begin{cases} \cos(m\phi) \\ \sin(m\phi) \end{cases}, \end{cases}$$

$$\begin{cases} \vec{E}_r^{\text{TM}_{mn}}(r, \phi) = -\bar{r}_0 B_{mn} \frac{1}{a} J'_m \left( \chi_{mn} \frac{r}{a} \right) \begin{cases} \cos(m\phi) \\ \sin(m\phi) \end{cases}, \\ \vec{E}_\phi^{\text{TM}_{mn}}(r, \phi) = \bar{\phi}_0 B_{mn} \frac{m}{\chi'_{mn} r} J_m \left( \chi_{mn} \frac{r}{a} \right) \begin{cases} \sin(m\phi) \\ \cos(m\phi) \end{cases}, \end{cases} \quad (4.19)$$

where  $m$  and  $n$  are integer azimuthal and radial wave indices, respectively;

$$A_{mn} = \left[ \frac{\varepsilon_m}{\pi(\chi_{mn}^2 - m^2)} \right]^{1/2} \frac{1}{J_m(\chi'_{mn})}, \quad B_{1n} = \left[ \frac{\varepsilon_m}{\pi} \right]^{1/2} \frac{1}{J_{m+1}(\chi_{mn})} \quad \text{are the}$$

normalization factors;  $J_m$  is the Bessel function of the first kind of the  $m$ -th order;  $\chi'_{mn}$  are the roots of the equation  $J'_m(\chi'_{mn}) = 0$ ;  $\chi_{mn}$  are the

roots of the equation  $J_m(\chi_{mn}) = 0$ ;  $\varepsilon_m = \begin{cases} 1 & \text{at } m = 0; \\ 0 & \text{at } m \neq 0. \end{cases}$

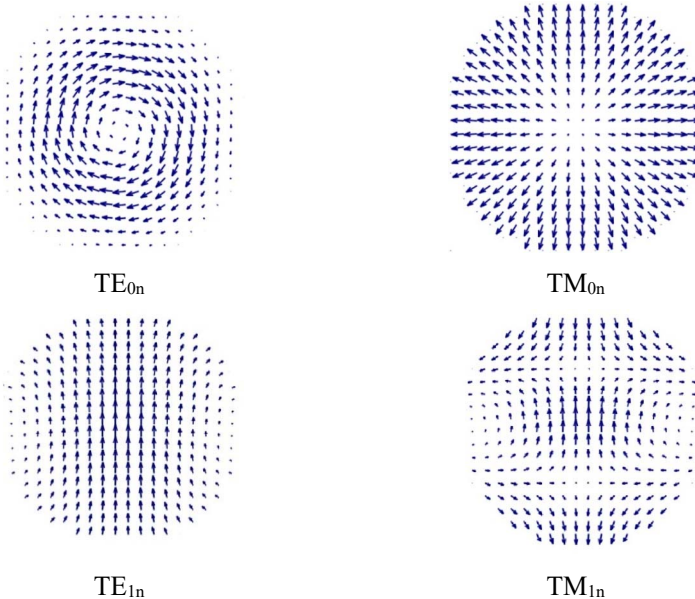


**Figure 4.38. The direction of the electric field vector for symmetric TE<sub>0n</sub>, TM<sub>0n</sub> and asymmetric TE<sub>1n</sub>, TM<sub>1n</sub> modes of a circular metal waveguide**

Using the Rayleigh-Sommerfeld integrals (4.1) and the well-known integral  $\int_0^{2\pi} \begin{Bmatrix} \cos(m\phi) \\ \sin(m\phi) \end{Bmatrix} \exp[-ix \cos(\phi - \theta)] d\phi = 2\pi(-i)^m J_m(x) \begin{Bmatrix} \cos(m\theta) \\ \sin(m\theta) \end{Bmatrix}$ , we find the field components of the investigated modes in free space at a distance  $z_1$  from the lens.

The field at the input and output of the lens with radius  $a_2$  is described using the phase correction function [148]. Again, applying the integral Rayleigh-Sommerfeld transformations (4.1) to the components of the electric field strength vector found after phase correction, we obtain analytical expressions for the transverse and longitudinal components of the given mode field at a distance  $z_2$  from the lens.

In the radially polarized  $TM_{01}$  mode, only the angular component of the field  $E_\phi(\rho_2, \theta_2, z_2)$  is missing, and the other two, including the longitudinal one, are nonzero. The field components for a radially polarized symmetric  $TM_{01}$  mode at a distance  $z_2$  from the lens have the form:

$$\left\{ \begin{array}{l} E_r(\rho_2, \theta_2, z_2) = \frac{k^2 z_1 z_2}{\xi_2^2} e^{ik\xi_2} B_{01} \frac{1}{a_1} \int_0^{a_2} \frac{e^{ik\xi_1}}{\xi_1^2} \int_0^{a_1} J_1\left(\chi_{01} \frac{r}{a_1}\right) \times \\ \times J_1(\gamma_1 r) \exp\left(\frac{ikr^2}{2\xi_1}\right) r dr J_1(\gamma_2 \rho_1) \exp\left(\frac{ik\rho_1^2}{2\xi_2}\right) Ph(\rho_1) \rho_1 d\rho_1 \\ E_\phi(\rho_2, \theta_2, z_2) = 0, \\ E_z(\rho_2, \theta_2, z_2) = \frac{ik^2 z_1}{\xi_2^2} \exp(ik\xi_2) B_{01} \frac{1}{a_1} \int_0^{a_2} \frac{e^{ik\xi_1}}{\xi_1^2} \int_0^{a_1} J_1\left(\chi_{01} \frac{r}{a_1}\right) \times \\ \times J_1(\gamma_1 r) \exp\left(\frac{ikr^2}{2\xi_1}\right) r dr [\rho_1 J_0(\gamma_2 \rho_1) + i\rho_2 J_1(\gamma_2 \rho_1)] \times \\ \times \exp\left(\frac{ik\rho_1^2}{2\xi_2}\right) Ph(\rho_1) \rho_1 d\rho_1. \end{array} \right. \quad (4.20)$$

The field components for an azimuthally polarized symmetric  $TE_{01}$  mode at a distance  $z_2$  from the lens have the form:

$$\left\{ \begin{array}{l} E_r(\rho_2, \theta_2, z_2) = 0, \\ E_\phi(\rho_2, \theta_2, z_2) = -\frac{k^2 z_1 z_2}{\xi_2^2} \exp(ik\xi_2) A_{01} \int_0^{a_2} \frac{e^{ik\xi_1}}{\xi_1^2} \int_0^{a_1} J_1\left(\chi_{01} \frac{r}{a_1}\right) \times \\ \times J_1(\gamma_1 r) \exp\left(\frac{ikr^2}{2\xi_1}\right) r dr J_1(\gamma_2 \rho_1) \exp\left(\frac{ik\rho_1^2}{2\xi_2}\right) Ph(\rho_1) \rho_1 d\rho_1, \\ E_z(\rho_2, \theta_2, z_2) = 0. \end{array} \right. \quad (4.21)$$

Note that the azimuthally polarized  $TE_{01}$  mode has only one angular component of the field  $E_\phi(\rho_2, \theta_2, z_2)$ , and the radial and longitudinal are equal to zero.

Field components for asymmetric modes  $TE_{11}$  and  $TM_{11}$  have the form:

$$\left\{ \begin{array}{l} E_r(\rho_2, \theta_2, z_2) = \frac{k^2 z_1 z_2}{\xi_2^2} \exp(ik\xi_2) A_{11} \sin(\theta_2) \int_0^{a_2} \left[ I_1(r) J_1'(\gamma_2 \rho_1) - I_2(r) \frac{J_1(\gamma_2 \rho_1)}{\gamma_2 \rho_1} \right] \times \\ \times \exp\left(\frac{ik\rho_1^2}{2\xi_2}\right) Ph(\rho_1) \rho_1 d\rho_1, \\ E_\phi(\rho_2, \theta_2, z_2) = \frac{k^2 z_1 z_2}{\xi_2^2} \exp(ik\xi_2) A_{11} \cos(\theta_2) \int_0^{a_2} \left[ I_1(r) J_1'(\gamma_2 \rho_1) - I_2(r) \frac{J_1(\gamma_2 \rho_1)}{\gamma_2 \rho_1} \right] \times \\ \times \exp\left(\frac{ik\rho_1^2}{2\xi_2}\right) Ph(\rho_1) \rho_1 d\rho_1 \\ E_z(\rho_2, \theta_2, z_2) = -\frac{k^2 z_1}{\xi_2^2} \exp(ik\xi_2) A_{11} \sin(\theta_2) \int_0^{a_2} \left[ iI_1(r) r J_1(\gamma_2 \rho_1) + I_1(r) J_1'(\gamma_2 \rho_1) + \right. \\ \left. + I_2(r) \frac{J_1(\gamma_2 \rho_1)}{\gamma_2 \rho_1} \right] \exp\left(\frac{ik\rho_1^2}{2\xi_2}\right) Ph(\rho_1) \rho_1 d\rho_1, \\ I_1(r) = \frac{\exp(ik\xi_1)}{\xi_1^2} \int_0^{a_1} \left[ \frac{1}{r} J_1\left(\chi_{11} \frac{r}{a_1}\right) J_1'(\gamma_1 r) + \frac{\chi_{11}}{a_1 \gamma_1 r} J_1'\left(\chi_{11} \frac{r}{a_1}\right) J_1(\gamma_1 r) \right] \exp\left(\frac{ikr^2}{2\xi_1}\right) r dr, \\ I_2(r) = \frac{\exp(ik\xi_1)}{\xi_1^2} \int_0^{a_1} \left[ \frac{1}{\gamma_1 r^2} J_1\left(\chi_{11} \frac{r}{a_1}\right) J_1(\gamma_1 r) + \frac{\chi_{11}}{a_1} J_1'\left(\chi_{11} \frac{r}{a_1}\right) J_1'(\gamma_1 r) \right] \exp\left(\frac{ikr^2}{2\xi_1}\right) r dr \end{array} \right. \quad (4.22)$$

$$\left. \begin{aligned}
 E_r(\rho_2, \theta_2, z_2) &= \frac{k^2 z_1 z_2}{\xi_2^2} \exp(ik\xi_2) B_{11} \cos(\theta_2) \int_0^{a_2} \left[ I_1(r) J_1'(\gamma_2 \rho_1) + I_2(r) \frac{J_1(\gamma_2 \rho_1)}{\gamma_2 \rho_1} \right] \times \\
 &\quad \times \exp\left(\frac{ik\rho_1^2}{2\xi_2}\right) Ph(\rho_1) \rho_1 d\rho_1, \\
 E_\phi(\rho_2, \theta_2, z_2) &= \frac{k^2 z_1 z_2}{\xi_2^2} \exp(ik\xi_2) B_{11} \sin(\theta_2) \int_0^{a_2} \left[ I_1(r) \frac{J_1(\gamma_2 \rho_1)}{\gamma_2 \rho_1} J_1'(\gamma_2 \rho_1) - I_2(r) J_1'(\gamma_2 \rho_1) \right] \times \\
 &\quad \times \exp\left(\frac{ik\rho_1^2}{2\xi_2}\right) Ph(\rho_1) \rho_1 d\rho_1 \\
 E_z(\rho_2, \theta_2, z_2) &= -\frac{k^2 z_1}{\xi_2^2} \exp(ik\xi_2) B_{11} \cos(\theta_2) \int_0^{a_2} \left[ iI_1(r) r J_1(\gamma_2 \rho_1) + I_1(r) J_1'(\gamma_2 \rho_1) - \right. \\
 &\quad \left. - I_2(r) \frac{J_1(\gamma_2 \rho_1)}{\gamma_2 \rho_1} \right] \exp\left(\frac{ik\rho_1^2}{2\xi_2}\right) Ph(\rho_1) \rho_1 d\rho_1, \\
 I_1(r) &= \frac{\exp(ik\xi_1)}{\xi_1^2} \int_0^{a_1} \left[ \frac{1}{a_1} J_1' \left( \chi_{11} \frac{r}{a_1} \right) J_1'(\gamma_1 r) + \frac{1}{\chi_{11} r} J_1 \left( \chi_{11} \frac{r}{a_1} \right) J_1(\gamma_1 r) \right] \exp\left(\frac{ikr^2}{2\xi_1}\right) r dr, \\
 I_2(r) &= \frac{\exp(ik\xi_1)}{\xi_1^2} \int_0^{a_1} \left[ \frac{1}{a_1} J_1 \left( \chi_{11} \frac{r}{a_1} \right) J_1(\gamma_1 r) + \frac{1}{\chi_{11} r} J_1 \left( \chi_{11} \frac{r}{a_1} \right) J_1'(\gamma_1 r) \right] \exp\left(\frac{ikr^2}{2\xi_1}\right) r dr.
 \end{aligned} \right\} \quad (4.23)$$

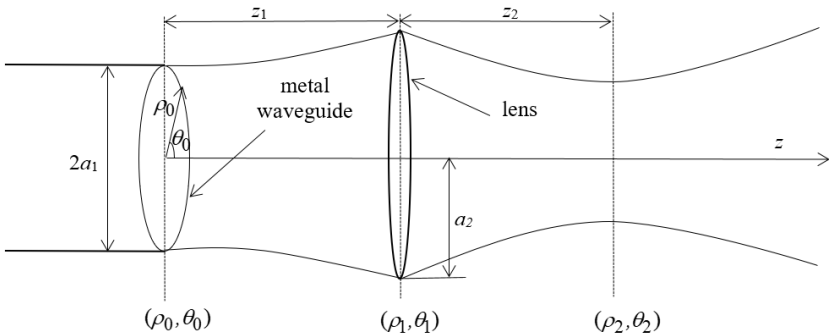


Figure 4.39. Theoretical scheme of the calculation model

The asymmetrical modes  $TE_{11}$  and  $TM_{11}$  contain all three field components.

### 4.3.2. Comparison of Experimental and Numerical Results

Using the obtained expressions (4.21–4.23), we calculated the transverse distributions of the total field intensity  $I(\rho_2, \theta_2, z_2) = |E_r|^2 + |E_\phi|^2 + |E_z|^2$  and the intensity of its longitudinal components of the resonator modes under study in the region of the minimum size of the focal spot of the focused radiation beams. The focal length of the lens  $F$  was chosen according to the conditions at moderate ( $NA = 0.16$ ) and at sharp focusing ( $NA = 0.68$ ). The wavelength of the radiation was chosen in the middle part of the terahertz range  $\lambda = 0.4326$  mm (the generation line of a THz laser with optical pumping on the HCOOH molecule). The diameter of the metal waveguide was chosen equal to  $2a_1 = 20$  mm. Calculations were carried out at  $\theta = \pi/2$ .

Figures 4.40 – 4.41 show the field intensity distributions for symmetric azimuthally polarized  $TE_{01}$  and radially polarized  $TM_{01}$  modes at moderate and at sharp focusing.

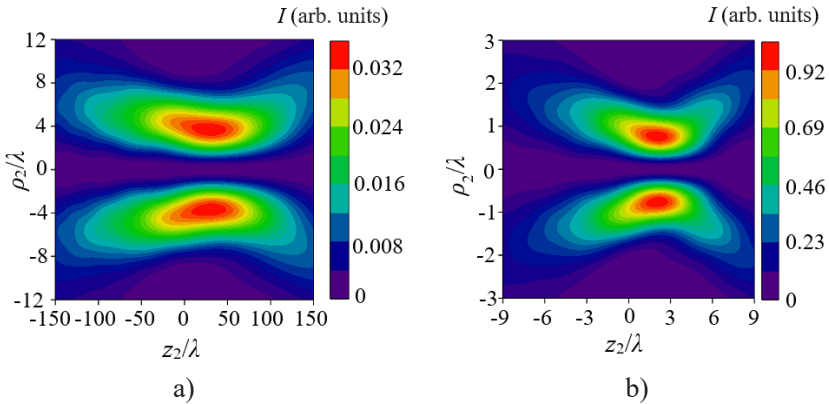


**Figure 4.40. Theoretical dependences of the total intensity of the field for the  $TE_{01}$  mode in the focal region of the lens at moderate (a) and at sharp (b) focusing**

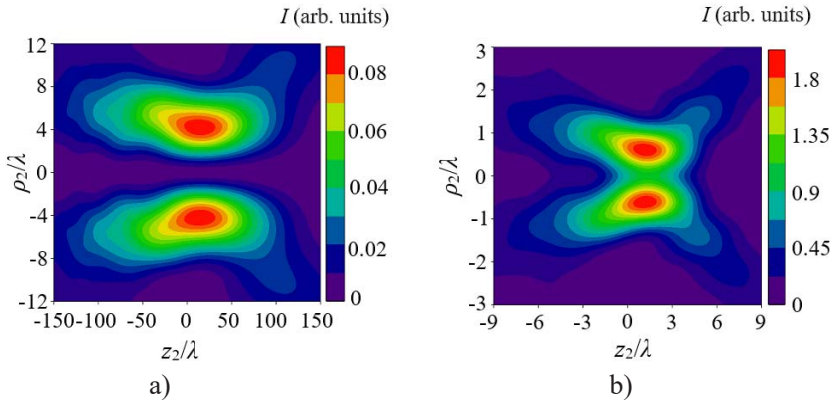


**Figure 4.41. Theoretical dependences of the total intensity of the field for the  $TM_{01}$  mode in the focal region of the lens at moderate (a) and at sharp (b) focusing**

Note some characteristic features. The transverse distribution of the total intensity of the field of the azimuthally polarized  $TE_{01}$  mode of the dielectric waveguide resonator in the region of the minimum size of the focused radiation beams retains an annular form (Figure 4.40) at both moderate and sharp focusing. The diameter of the beam of this mode at the focus of the lens at moderate focusing was  $FWHM = 10.8 \lambda$ , and at sharp focusing was  $FWHM = 2.5 \lambda$ , which completely coincides with the azimuthally polarized  $TE_{01}$  mode of the dielectric resonator.

For the radially polarized  $TM_{01}$  mode, at sharp focusing, a significant increase in axial intensity is observed in the transverse distribution of the field (Figure 4.41 b), which is absent at moderate focusing (Figure 4.40 a). This is explained by the fact that the longitudinal component of the  $TM_{01}$  mode has a field maximum on the beam axis (Figure 4.41). At the same time, the diameter of the  $TM_{01}$  mode beam at the focus of the lens at moderate focusing is equal  $FWHM = 9.9 \lambda$ , and at sharp focusing is  $FWHM = 2.2 \lambda$ .

Figures 4.43 – 4.46 show the distribution of the total field intensity, as well as the intensity of their longitudinal component for asymmetric  $TE_{11}$  and  $TM_{11}$  modes.

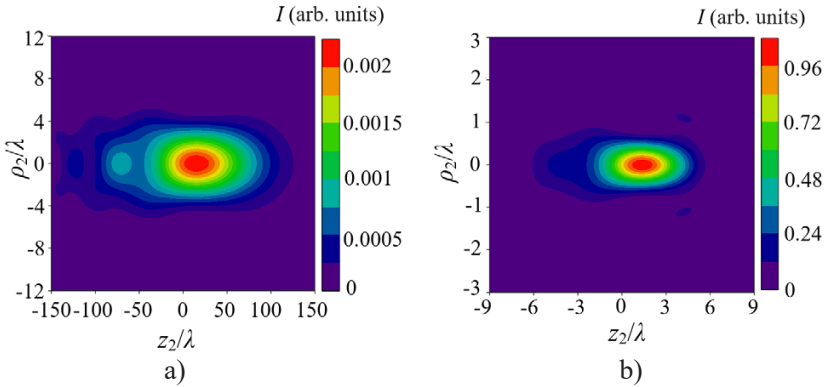


**Figure 4.42. Theoretical dependences of the intensity of the field of the longitudinal component for the  $TM_{01}$  mode in the focal region of the lens at moderate (a) and at sharp (b) focusing**

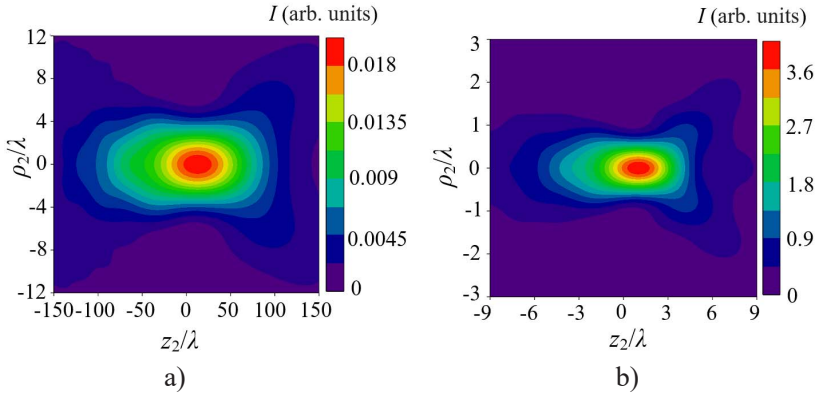


**Figure 4.43. Theoretical dependences of the total intensity of the field for the  $TE_{11}$  mode in the focal region of the lens at moderate (a) and at sharp (b) focusing**

It can be seen from the figures that the transverse distribution of the total field intensity for the  $TE_{11}$  mode has a maximum on the beam axis (Figure 4.43) with both types of focusing – moderate and sharp. The diameter of the  $TE_{11}$  mode beam at the focus of the lens at moderate focusing was

FWHM =  $4.5 \lambda$  and at sharp focusing was FWHM =  $0.97 \lambda$ . In the field distribution for the longitudinal component of this mode has a dip in the lens focus (Figure 4.44), but the contribution of this component to the total intensity is insignificant.

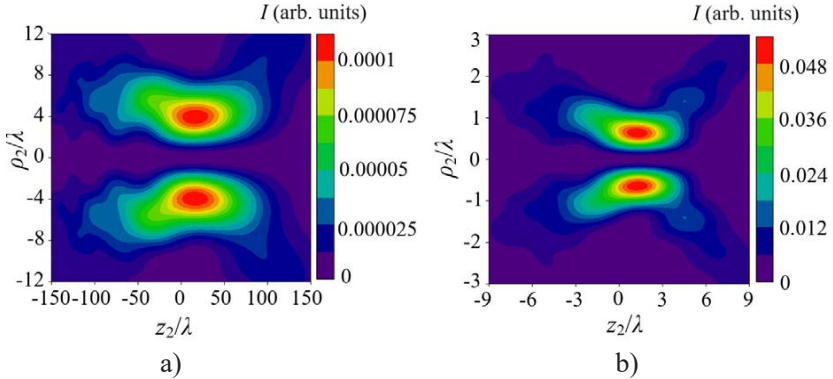


**Figure 4.44. Theoretical dependences of the intensity of the field of the longitudinal component for the  $TE_{11}$  mode in the focal region of the lens at moderate (a) and at sharp (b) focusing**

The transverse distribution of the total field intensity for the  $TM_{11}$  mode has a dip both at sharp and moderate focusing in the focal region (Figure 4.45). It can be observed that the side lobes of the field of this mode have different intensities. This can be explained by the fact that the maximum intensity of the field of the longitudinal component of the  $TM_{11}$  is shifted with both types of focusing (Figure 4.46). At the same time, the diameter of the  $TM_{11}$  mode beam in the focus of the lens at moderate focusing was FWHM =  $13.9 \lambda$ , and at sharp focusing was FWHM =  $3.4 \lambda$ .

The dependence of the relative contribution of the longitudinal component of the field of these modes to their full intensity on the numerical aperture of the lens was also studied. The calculation was carried out by the formula 3.11. The calculation results are shown in Figure 4.47. It can be seen that by increasing the numerical aperture, the contribution of the longitudinal component of the field for  $TM_{01}$  grows to 37 %,  $TE_{11}$  – 2 % and for  $TM_{11}$  mode to about 6 %.

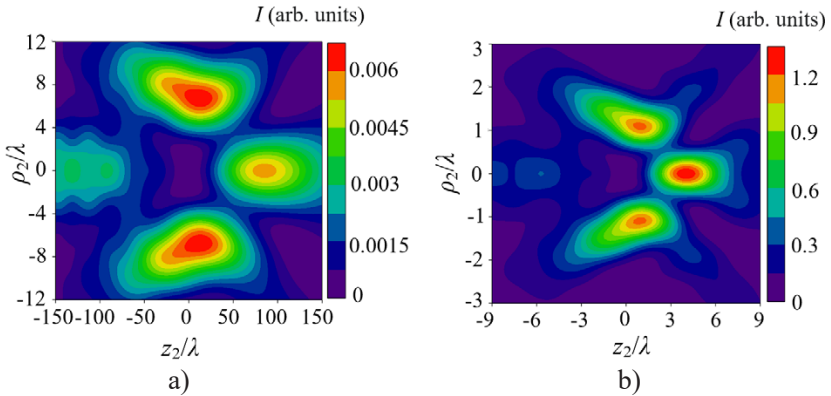


**Figure 4.45. Theoretical dependences of the total intensity of the field for the  $TE_{11}$  mode in the focal region of the lens at moderate (a) and at sharp (b) focusing**

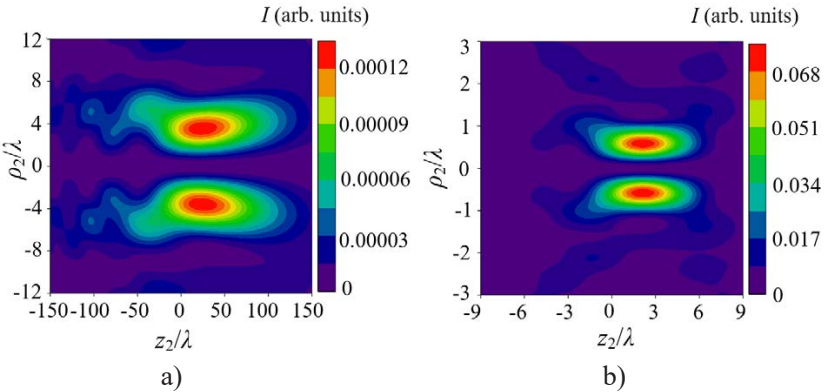


**Figure 4.46. Theoretical dependences of the intensity of the field of the longitudinal component for the  $TM_{11}$  mode in the focal region of the lens at moderate (a) and at sharp (b) focusing**

Next, we estimated the effect of the full intensity of the longitudinal components for different distances  $z$  ( $NA = 1$ ). Figure 4.48 illustrates the calculation results. It can be seen that the growth  $\eta$  is observed in a small local area with a center near the focal length of the lens.

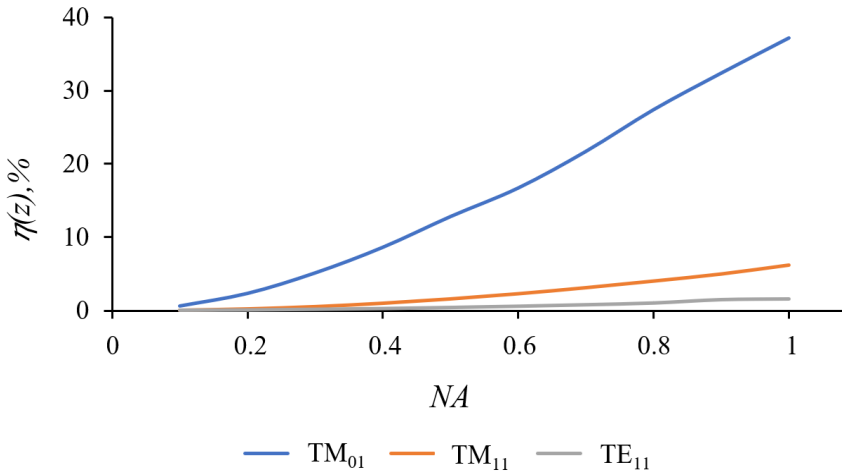


**Figure 4.47. Dependencies of the relative contribution of the longitudinal field component of  $TM_{01}$ ,  $TM_{11}$ , and  $TE_{11}$  modes to their total intensity at different values of the numerical aperture of the  $NA$  lens**

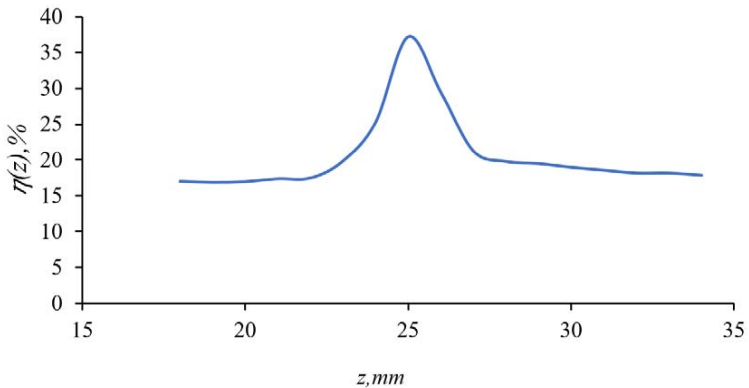


**Figure 4.48. Dependencies of the relative contribution of the longitudinal component of the  $TM_{01}$  mode field to the total intensity at sharp ( $NA = 1$ ) focusing in the focal region of the lens**